Biophysical Influence of Nanofiber Networks to Direct Pericyte Aggregation into Spheroids

Sharan Sharma

Thesis submitted to the faculty of the Virginia Polytechnic Institute and State University
in partial fulfillment of the requirements for the degree of

Master of Science
In
Mechanical Engineering

Amrinder S. Nain, Chair
Julie A. Phillippi
Mark R. Paul

May 02, 2023
Blacksburg, VA

Keywords: Spheroids, pericytes, nanofibers, forces, contractility

Biophysical Influence of Nanofiber Networks to Direct Pericyte Aggregation into Spheroids

Sharan Sharma

ABSTRACT

Multicellular spheroids have emerged as a promising tool for drug delivery, cancer therapy, and tissue engineering. Compared to 2D monolayers, spheroids provide a more realistic representation of the 3D cellular environment, enabling better understanding of the signaling cascades and growth factors involved in vivo. The formation of in vitro spheroids involves the aggregation of several cells that proliferate to grow into larger spheroids. Biophysical cues provide crucial information for the cells to assemble into 3D structures. We used suspended fiber networks to demonstrate a new way to form and spatially pattern spheroids comprised of human pericytes. We show that fiber architecture (aligned vs. crosshatched), diameter (200, 500, and 800 nm), and contractility influence spheroids in their spontaneous formation, growth, and maintenance, and report a dynamic trade of cells between adjacent spheroids through remodeled fiber networks. We found that aligned fiber networks promoted spheroid formation independent of fiber diameter, while large-diameter crosshatched networks abrogated spheroid formation, promoting growth of 2D monolayers. Thus, a mixture of diameters and architectures allowed for spatial patterning of spheroids and monolayers within a single system. We further quantified various dynamic interactions and describe the forces involved during spheroid formation, cell efflux from spheroids, and show the loss and recovery of spheroid forces with pharmacological perturbation of Rho-associated protein kinase (ROCK). Thus, we develop new insights on the dynamics of spheroids

using suspended fiber networks of varying diameters and architectures, with the potential to connect matrix biology with developmental, disease, and regenerative biology.

Biophysical Influence of Nanofiber Networks to Direct Pericyte Aggregation into Spheroids

Sharan Sharma

GENERAL AUDIENCE ABSTRACT

In recent years, studies involving multicellular spherical aggregates or 'spheroids' have gained popularity since they capture the 3D cellular environments seen within the body more realistically when compared to 2D cell culture systems (such as monolayers) traditionally used for biological studies. These spheroids resemble organs and tissues in terms of their structure and function better and are increasingly being studied for an array of applications such as drug delivery, cancer therapy, as implants and in tissue regeneration and tissue engineering. The cellular microenvironment consists of fibrous proteins of varying diameter arranged in various geometric patterns, which can influence the growth and culture of spheroids. Here, we use our Spinneret-Based Tunable Engineered Parameters (STEP) technique to fabricate fibrous networks with precise control over fiber diameter and architecture and study how biophysical cues can influence the formation and culture of spheroids. Using aortic pericytes, we show that fiber architecture (aligned vs. crosshatched) and diameter (200, 500, and 800 nm) can control how pericytes aggregate into either 2D monolayers or 3D spheroids. We study the effect of each of these parameters to show that stiffer, denser fibers are robust networks which the cells refrain from remodeling, and thus lead to monolayers while more compliant and sparser networks are easily remodeled to promote spheroid formation. Thus, we spatially pattern a mixture of 3D spheroids and 2D monolayers in a single system by varying the parameters at different regions. We quantify various interactions such as spheroid

formation, spheroid merging, spheroid migration, cell efflux from spheroids and the dynamic contractile forces exerted on the matrix by spheroids during these interactions. We also show that contractility has a major role in spheroid formation and to maintain their structure and look at the changes in the gene expressions associated with contractility during the formation and growth of spheroids. Thus, we develop new knowledge in controlling the growth of pericytes into 2D and 3D structures and show that our fiber networks can be an essential platform for studying spheroids.

Acknowledgements

First and foremost, I would like to thank my advisor, Dr. Amrinder Nain, for his constant support and guidance throughout my journey. Dr. Nain has not just been a great academic advisor, but also an excellent mentor and a good friend. I have improved tremendously both professionally and as a person during my time in the lab and I have a great understanding of my path moving ahead.

I would like to thank Dr. Phillippi for her tremendous contributions to my research, her advice with planning my experiments, interpreting data, and writing have been extremely helpful and has made me a better researcher. I would also like to thank Dr. Paul for serving on my committee.

The help and support from all the STEP lab members have been great and is what kept me going during difficult times. Abinash, Aniket, and Appy were very helpful during my initial stages, and have my respect for taking time to train me during their final years with their hectic schedules. I enjoyed spending time with Christian, Atharva, Harsimran, and Ishanee, who were always available, either for guidance and support or for the many random conversations, and I cannot imagine this journey without them.

I would also like to extend my gratitude to my family and friends. My family has been a constant source of advice and always supported my decisions. My friends, old and new, helped me make this transition and journey smooth, memorable, and fun.

Finally, I would like to thank Virginia Tech for providing me with a platform to improve as an engineer, with its wonderful staff and facilities without which none of this would have been possible. I thoroughly enjoyed my time here and it has helped me improve in all aspects of life.

Table of Contents

List of Figures

List of Tables

1 Introduction

1.1 Three-dimensional culture systems and their advantages over two-dimensional culture systems

Cells exhibit fundamental behavioral differences when cultured on two-dimensional (2D) flat substrates versus three-dimensional (3D) culture systems.[1–3] Culture systems can differentially influence various properties like cell morphology, cellular responses such as migration, proliferation and adhesion, and genetic expression.[1,4] 2D substrates generally tend to be more stiff when compared with *in vivo* microenvironments and they lack many of the biophysical and biochemical properties crucial for mimicking cellular function.[3,5] 3D cell culture systems more completely capture the functional and architectural characteristics of native tissues by having controllable features such as biophysical and biochemical gradients directing cell-cell and cell-substrate interactions that represent either physiological or pathological environments.[4–6]

3D multicellular spherical aggregates of cells, termed *spheroids* have become increasingly popular in vitro platforms due to their ability to recover *in vivo* characteristics that standard 2D culture platforms fail to do.[5,7–10] Spheroids are considered better representative of cells within the *in vivo* tissue microenvironment than 2D monolayer cultures in multiple and varied ways such as mechanical force exertion, biophysical and biochemical signaling, and electrical coupling to influence morphology, motility, proliferation, differentiation, and genetic expression.[5] The self-assembly of spheroids from individual, dispersed cells is known to replicate multiple processes that occur during embryogenesis, morphogenesis and organogenesis and can give insights

into the interaction between cells and external environment during early stages of development.[5],[3] Spheroids are also known to maintain the functionality and characteristics similar to tissues for longer duration.[9] Tumor cell-derived spheroid models are also popular for studying cell behavior and determining the effect of putative therapeutic drugs.[2–5] Because of these advantages, spheroids are increasingly being used for applications such as tissue engineering, regenerative medicine, drug development and screening, and single- and multi-organ-on-a-chip devices integrated with microfluidics.[2,3,9]

1.2 Methods to grow spheroid cultures

Over the years, multiple methods have been established to induce and culture spheroids of different pluripotent and adult tissue cell lineages such as human umbilical vein endothelial cells, human mesenchymal stem cells, chondrocytes, dermal fibroblasts, murine embryonic stem cells, and those from various tumors such as colon, breast, pancreas, and brain.[3,6,11] Spheroids can be grown in scaffold-free cell suspension systems such as on anti-adhesion substrates or using the hanging drop method.[9] Various techniques such as microfluidics, rotating wall vessels, spinner culture, pellet culture, and liquid overlays have also been developed to induce spheroids.[6,9] Many studies have also shown controlled and consistent spheroid growth of uniform size.[9] Spheroids can also be grown in scaffold based systems such as fibrous hydrogels, natural extracellular matrix, and other polymer-based matrices.[5,6,9,12]

1.3 Mechanobiology of multicellular spheroids

Multiple studies have revealed the mechanobiological underpinnings of spheroid formation,[13] growth, and subsequent interactions with the surrounding fibrous microenvironment.[14–19] Spheroids can be classified with distinct zones, with a central core where the cells are densely packed and an invasive zone around the boundaries where cells try to migrate out of the spheroid.[20–22] Cell-cell interactions dominate in the core while the invasive population has increased cell-ECM interactions. These regions are not just distinct spatially, they also have different chemoresistance and tolerances to drug treatments.[21] The invasive leader cells show different gene profiling when compared to detached cells around the spheroid, indicating distinct signaling mechanisms for these phenomena.[23] Invasion (or sprouting) of cells occur through the degradation and remodeling of the surrounding matrix and the mechanical properties of the matrix can play a crucial role in controlling invasion. With endothelial cells, it was shown that increasing fiber stiffness promotes sprouting of cells while the pore density controls whether cells sprout in the form of leader/follower cells (small pore size) or as individual cells (large pore size).[21] By varying fibrinogen and thrombin concentrations, Dey *et al.* observed that changes in the fiber diameter, fiber crosslinking and stiffness influence the invasiveness and sprouting ability of cells from Human umbilical vein endothelial cell (HUVEC) spheroids.[24] Cells migrating away from the spheroids have been shown to be more deformable when compared to those at the spheroid surface in breast cancer spheroids, indicating the role of cell stiffness in detachment and migration of the cells from the spheorids.[25]

Spheroids can also have multiple migration modes[26] and their packing density can influence their migration speeds, with densely packed ovarian cancer spheroids showing early and faster migration compared to loosely packed ones.[22] Spheroid mergers are also of interest, with spheroids of either same or different cell line and area have been studied using different platforms.[27,28] Spheroids adjacent to each other show directional sprouting to form larger, more complex systems.[21] Various patterns can also be induced during mergers, with the spheroids manipulated using magnetic particles embedded into them.[29] Tumor spheroids were shown to engulf fibroblast spheroids during merging.[30] Multiple human hepatocyte spheroids were merged in a bioreactor to form tissue like structures, which maintained multiple functional features for up to 25 days.[31]

Another aspect of interest is the amount of contractile forces these spheroids exert on the surrounding matrix. Multiple methods have been developed to calculate the forces exerted by 2D cells, monolayers and 3D aggregates on the surrounding matrix such as monolayer stress microscopy, 2D, 2.5D and 3D traction force microscopy. Platforms have also been developed to calculate the internal stresses within the spheroid using FRET tension sensors, inclusions, laser ablations, etc.[32] Within the spheroid, higher compressive stress regions are associated with decreased proliferation and increased apoptosis; with cancer cells possibly identifying low stress regions to escape from a spheroid.[21] External forces also influence spheroid behavior. Endothelial cell spheroids showed sprouting along the fibers when mechanical forces were induced in those fibers.[21] Most of these dynamic interactions involve the surrounding matrix and multiple studies have reported fiber remodeling around spheroids. Tenocyte spheroids showed contraction and alignment of the collagen fibers around them in the presence of low serum media and

growth factors.[21] In MDA-MB-231 spheroids, sprouting involved deformation and reorganization of collagen fibers.[23] The transcriptional gene profiles in tumor angiogenesis and cancer invasion were also impacted by the extracellular matrix and the stromal cell density.[24] With hMSCs spheroids, it was shown that fiber remodeling via cell forces helps cells directionally move towards spheroids.[33]

Introduction of fibers into spheroid cultures can enhance their formation and size,[34] and has shown to increase cell-cell interactions, facilitate important cell-ECM interaction during aggregation and provide mechanical strength to the spheroids.[35,36] Increased tension in the fibers has been shown to increase capillary sprouting of endothelial cell spheroids,[15] while increasing matrix stiffness can increase invasiveness of endothelial and pericyte spheroids.[14,37] Spheroids have also been shown to exert large contractile forces and deform the surrounding matrix.[38] Thus studying how the biophysical aspects of the surrounding matrix influences spheroid formation and their dynamic interactions with the fibers are crucial in understanding spheroid behavior and function

1.4 Three-dimensional aggregation of pericytes

Pericytes are mural cells and are predominantly found in the microvasculature with crucial roles in vascular formation and maintenance.[39–41] They are usually embedded in the vessel basement membrane, where they surround endothelial cells and have been shown to modulate blood flow, vessel wall tension and regulate vessel wall diameter and blood flow rate via active contraction and dilation at different time scales.[41] Members of our team have previously demonstrated that human pericytes derived from vasa vasorum spontaneously self-assemble into spheroids when cultured on Matrigel substrates.[42] Human brain microvascular pericytes have been shown to form spheroids when

cocultured with other cells such as endothelial cells, astrocytes and used to study cell behavior for tissue engineering and drug delivery.[43–45] With human brain pericyte spheroids, it was shown that Notch3 (which is required to maintain pericyte populations[46]) silencing increased pericyte outgrowth into the surrounding collagen matrix while overexpression had the opposite effect.[47] Primary pericytes isolated from mouse lungs were shown to respond to mechanical stimuli, with increase in stiffness inducing morphological changes, differentiation into a fibroblastic phenotype and increasing the invasiveness of pericyte spheroids.[14] Thus, changing the mechanical properties of the matrices may influence pericyte behavior and aggregation.

1.5 Objectives of this study

How fiber size, fiber network architecture, and alignment can influence spheroid formation, growth, and behavior and how multiple spheroids interact with each other through the surrounding matrix remains largely unknown. Here, we use tunable 3D fiber networks as a platform to study the biophysical influence of the underlying microenvironment on pericyte spheroids. We inquired if fiber dimension and their architecture regulate aggregation of cells into spheroids and affected their size, shape, and dynamics. We also capture various dynamic interactions of the spheroids with individual cells, spheroids, and fibers, with the fiber networks proving an effective tool to study their behavior in matrix environments. Using quantitative microscopy, we measure forces involved during formation of spheroids, when individual cells sprout out of the spheroid, their migratory patterns, and study fiber diameter and architecture dependent spatial patterning of spheroids. Overall, we develop new knowledge in the 3D dynamics of

spheroids that may connect matrix biology with developmental, disease, and regenerative biology.

1.6 Materials and methods

1.6.1 Fiber network manufacturing and characterization:

To create the suspended fiber networks, a non-electrospinning technique called STEP technique was used on flat, hollow metal scaffolds. This technique allows for control over fiber diameter, spacing, and architecture.[48] Polystyrene (MW: 2,500,000 g/mol; CAS No. 1025; Scientific Polymer Products, Ontario, NY, USA) was dissolved in xylene (CAS No. 1330-20-7; Carolina, Burlington, NC). And then extruded using a micropipette (Jensen Global, Santa Barbara, CA, USA). Aligned fiber networks were created by depositing base fibers which were around 2 µm thick and spaced about 350 µm apart, followed by orthogonal layers of fibers with diameters of approximately 200/500/800 nm and spacing of approximately 10 µm. Crosshatch fiber networks involved two densely spaced orthogonally deposited layers of fibers with the same diameter of 200/500/800 nm. The intersections were fused using Tetrahydrofuran vapors to preserve their architecture. Scanning electron microscopy (SEM) (JSM-IT500 InTouchScope™ Scanning Electron Microscope (JEOL Ltd., Akishima, Tokyo, Japan)) was used to characterize the fiber networks.

1.6.2 Cell culture on nanofiber scaffolds

The fiber networks were placed in 6-well plates (CAS No. P06-1.5H-N; Cellvis, Mountain View, CA), treated for 10 mins with 70% ethanol for sterilization and washed twice with PBS. 4 µg/mL Fibronectin (CAS No. F1141-1MG; MilliporeSigma,

Burlington, MA, USA) incubated for 45 mins at 37°C was used to functionalize the fibers and glass to facilitate cell adhesion. Human pericytes were derived the adventitia of ascending aorta, resected during heart transplantation operations with approval from the Institutional Review Board (University of Pittsburgh Protocol #PRO20040179) under an informed consent process, isolated, and subsequently culture expanded as previously described.[42] StemMACS™ MSC Expansion Media (Order No. 130-091-680; Miltenyi Biotec, North Rhine-Westphalia, Germany) was used to culture-expand the pericytes and a HPV E6/E7 lentiviral system as previously reported[49] was used to immortalize them. From passages 70-85, 0.1% Trypsin-EDTA (CAS No R001100; ATCC, Manassas, VA) was used to detach the cells and seed on fiber networks. After allowing the cells to adhere to the fiber for 30-45 minutes at 37°C and 5% CO_2, 3 mL of culture medium was added to flood the wells. For the first two weeks, the culture media was replenished every week and subsequently for the next two weeks, media was changed every 2-3 days. To inhibit actin-myosin mediated contractility through the inhibition of Rho-associated protein kinase (ROCK), the cells were also cultured with 10 µM and 20 µM of a chemical antagonist, Y-27632 (HB2297, Hello Bio Inc, Princeton, NJ) dissolved in PBS. The existing culture media with the drug was pipetted out and the wells were washed twice with 1 mL of the culture media for y-27632 drug wash out, followed by addition of 3 mL of fresh culture media.

1.6.3 Time-lapse, epifluorescence, and confocal microscopy

Time lapse videos were taken after placing the 6-well plates in an AxioObserver Z1 (Carl Zeiss, Jena, Germany) microscope with a 20x objective at 5- or 10-min intervals. To image the entire scaffold, mosaic images were taken with this objective. To fix cells and

spheroids, 4% paraformaldehyde was used followed by permeabilization with 0.1% Triton X100 solution and blocking with 5% goat serum before being stained for nuclei (DAPI (Invitrogen)), F-actin stress fibers (Phalloidin (Alexa Fluor™ Plus 647 Phalloidin, Invitrogen)), while the fibers were stained before seeding by incubating with Rhodamine Fibronectin (Cytoskeleton Inc.) for 1 hour at 37°C and 5% CO_2. Stained spheroids were imaged in an LSM 880 confocal microscope (Carl Zeiss, Jena, Germany).

1.6.4 RNA isolation and gene expression analysis

Cells and spheroids cultured on fiber networks were lysed at weekly intervals for three weeks. NucleoSpin® RNA kit (Takara/Clontech 740955) was used to isolate total RNA, which was followed by cDNA synthesis with High Capacity cDNA Reverse Transcription kit (ThermoFisher 4368814) and quantification using Qubit™ ssDNA Assay (ThermoFisher Q10212), following manufacturers' instructions. 10ng (Sm22, Smtn, PPIA) or 100ng (Acta2, Cnn1) cDNA inputs were used for qPCR using Taqman™ technology (ThermoFisher 4369016; refer to Table 1 for primer/probe details) and a QuantStudio™ 3 thermal cycler (ThermoFisher A28131). StepOne Plus v 2.2 software was utilized for data analysis; amount of gene expression normalized to the housekeeping gene PPIA was calculated using the $2^{-\Delta Ct}$ method.

Table 1.1: Taqman primer/probe sets

Target	Catalog Number
Acta2	Hs00909449_m1
Cnn1	Hs00154543_m1
Sm22	Hs01038777_g1
Smtn	Hs00199489_m1
PPIA	Hs99999904_m1

1.6.5 Quantitative analysis of cells and spheroids

Cells and spheroids were quantitatively analyzed using ImageJ (NIH; https://imagej.nih.gov/ij/). Boundaries of cell and spheroid were outlined manually to extract data such as area, circularity, and aspect ratios. Using nanonet force microscopy technology[50–53] forces exerted by the cells and spheroids on the aligned fiber networks were estimated. The stiff base fibers act as fixed boundary conditions while the thinner aligned fibers fused to these on both sides act as fixed-fixed beams. The force exerted on the fibers is calculated by estimating the deflection of the fiber by the cell/spheroid. Migration rates were quantified by tracking the centroid. Persistence was computed as the ratio of the total displacement of the cell/spheroid to the total distance travelled. By tracing the nuclear and spheroid boundary from confocal z-stack images, their polarities were compared. The difference between the major axes of both boundaries (an angle between 0° and 90°) was estimated. Student's t-tests were used for statistical analysis, with a p value < 0.05 classified as *, <0.01 as **, and <0.001 as ***.

2 **Results**

2.1 Pericytes self-assemble into spheroids when seeded on suspended fiber networks

We wanted to inquire if cells on suspended STEP fiber networks aggregated to form spheroids. We seeded pericytes on suspended fiber networks with aligned and crosshatched fiber architectures (**Figure 1a,b**) and varied the diameter of the fibers within these fused (**Figure 1c**) networks (200 nm, 500 nm, 800 nm, and 2000 nm, **Figure 1d**) to capture *in vivo* matrix dimensions.[54,55] Pericytes self-assembled into spherical multicellular aggregates or '*spheroids*' over a time scale of hours, once initiated (**Figure 2a**). These spheroids were formed when three or more cells interacted with each other simultaneously, collectively contracting over time (**Figure 2b**). Aortic pericytes derived from other patients either from the adventia or the placenta also showed spheroid formation on fiber networks (**Figure 2c-e**). To visualize their three-dimensional organization on fiber networks, we cultured spheroids on fibers coated with rhodamine-conjugated fibronectin. Confocal images of spheroids labelled with DAPI and phalloidin showed these spheroids to form around multiple fibers above and below the fiber plane. (

Figure 3a,b).

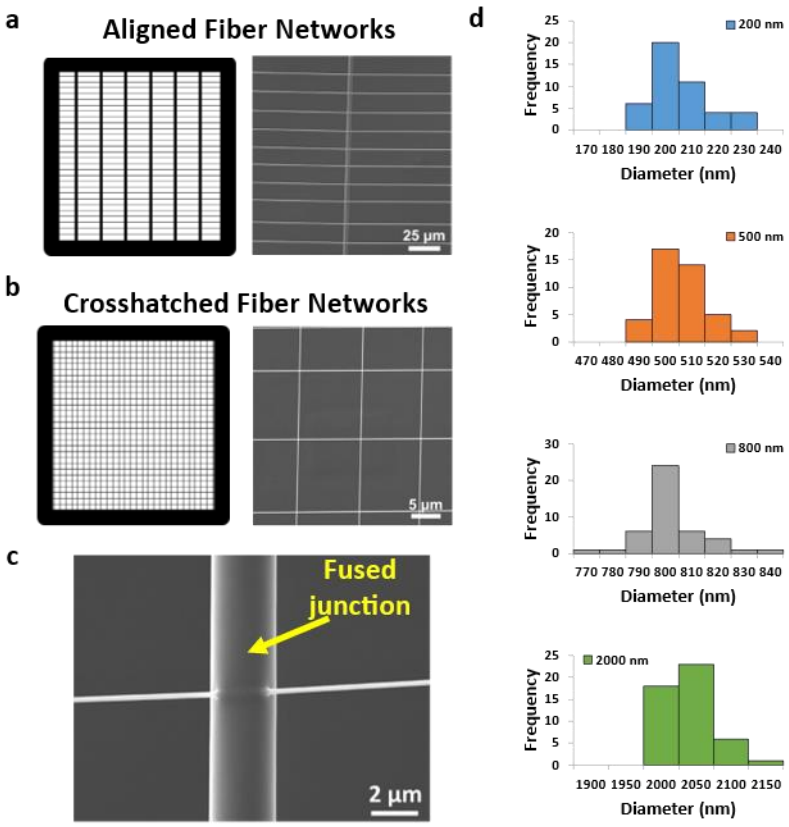

Figure 1: Representative image (left) and a SEM image of a zoomed in section (right) of (a) an aligned fiber network (Scale bar: 25 µm) (b) a crosshatched fiber network (Scale bar: 5 µm). (c) A SEM image of a junction where the two overlapping fibers are fused to each other (Scale bar: 2 µm). (d) Diameter measurements of the fabricated fibers of 200, 500, 800 and 2000 nm.

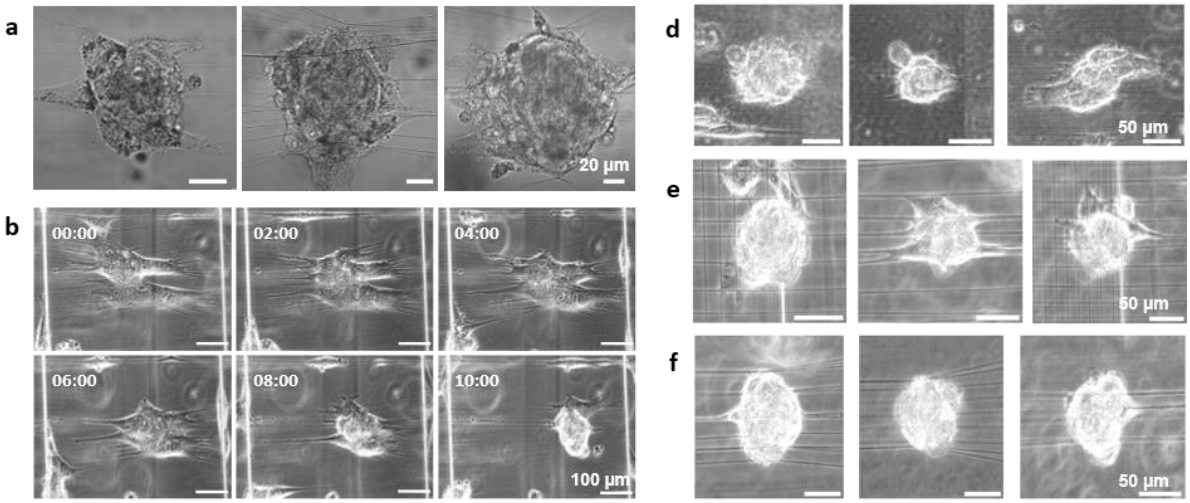

Figure 2: (a) Phase images of spheroids formed on aligned fiber networks (Scale bar: 20 µm). (b) Time lapse phase images of multiple pericyte cells forming a spheroid over 10 hours (Scale bar: 2 µm; Time scale: hr:min). (c-e) Spheroid formations with aortic pulmonary pericytes from different patients derived either from the adventia or the placenta on fiber networks (Scale Bar: 50 µm).

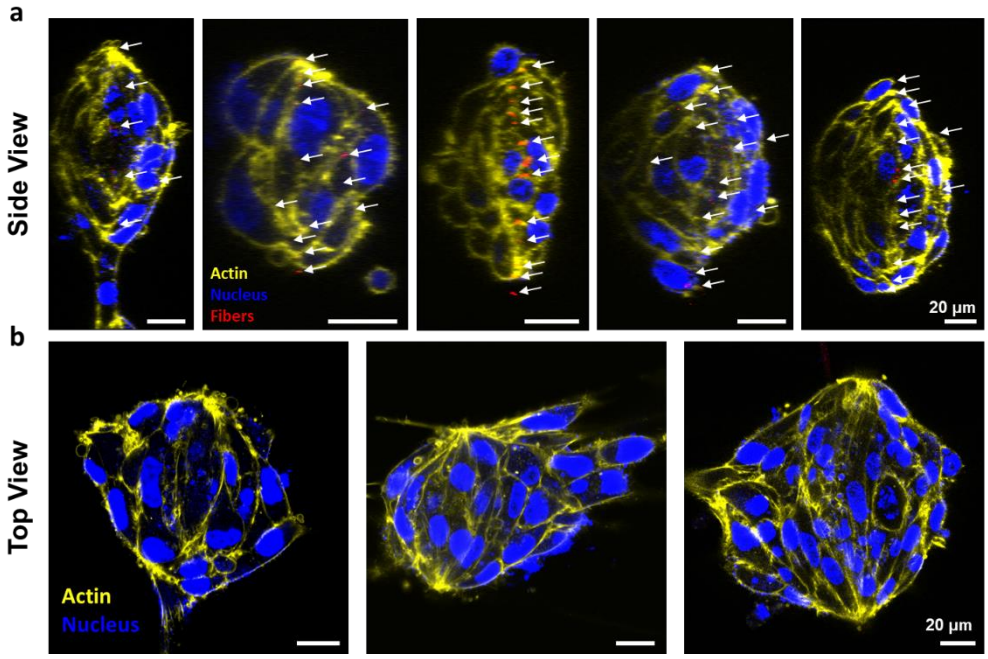

Figure 3: (a) Confocal images of cross section of spheroids formed on fiber networks. The arrow marks (white) indicate the position of the fibers (red) within the spheroids (Yellow: Actin, Blue: Nucleus, Red: Fibers, Scale bar 20 µm). (b) Confocal images of a section of the spheroids as seen from the top (Yellow: Actin, Blue: Nucleus, Scale bar: 2 µm).

To differentiate from individual cells or cell clusters, spheroids were classified with large areas (~6187.63 ± 3449.76 μm^2 (spheroids) vs. 1066.35 ± 832.35 μm^2 (cells)) and high circularities (~0.71±0.14 (spheroids) vs. 0.21 ± 0.08 (cells)) and were significantly different (P<.001) from single cells or small clusters of three or fewer cells (**Figure 4a**). Confocal images of spheroids showed that as spheroids grew in area, the number of cells within them increased linearly (**Figure 4b**). When comparing the angle between the major (long) axes of the nuclei with the major axis of the spheroid, 38% of the cells had a nuclear angle <15° while 60% of the cells had an angle <30°, indicating that the cells were polarized along with the spheroid. (**Figure 4c**)

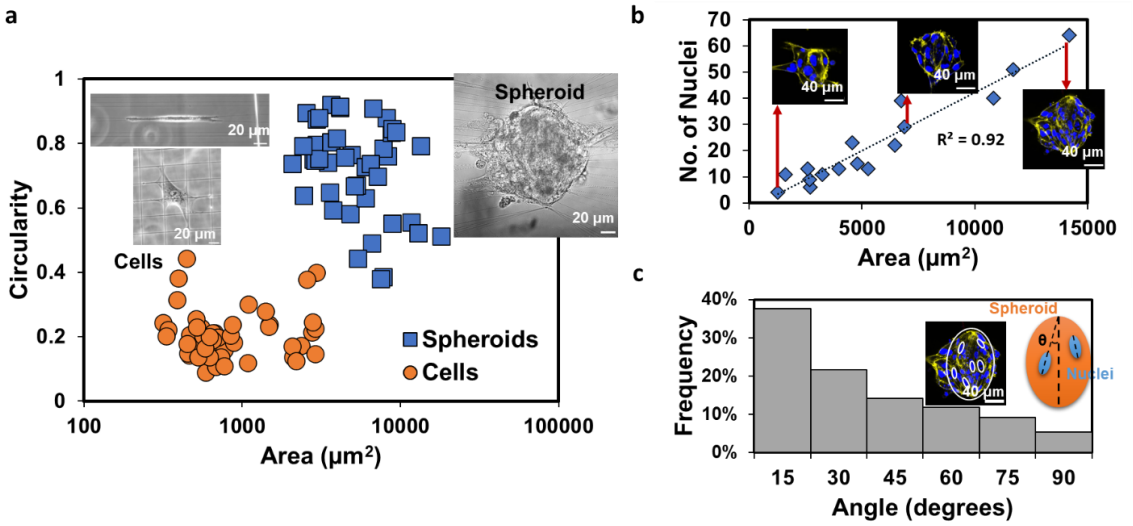

Figure 4: (a) Cells on fiber networks (inset, left, N=49) had lower circularities and smaller areas while spheroids (inset, right; N=49) were classified with high circularities and larger areas. (b) The number of nuclei (or cells) within the spheroid increases linearly with spheroid area (N=16). Inset: Top view images of spheroids stained for actin (yellow) and nucleus (blue) representing the marked points (red arrows) in the plot. (c) Nuclei within the spheroids have their major (long) axes aligned towards the major axis of the spheroid, indicated by the large number of nuclei having a small angle (0° - 30°) with the major axes of the spheroid and the nucleus (n=391 (nuclei), N=19 (spheroids)). Insets show a spheroid stained for actin (yellow) and nucleus (blue) and some nuclear boundaries marked in white (left) and a representative image showing the angle between the major axes of the spheroid and the nuclei (right).

2.2 Biophysical cues from the underlying microenvironment influence spheroid formation

We wanted to inquire if spheroid formation on fiber networks were influenced by the size and architecture of the underlying fiber networks. To do so, we cultured pericytes on STEP fiber networks of three different diameters and two architectures and tracked them for three weeks.

On aligned fiber networks, which had densely spaced (~10 μm) aligned fibers in one direction of either 200, 500 or 800 nm fused to orthogonal, sparsely spaced (~360 μm) thick (2 μm) fibers, spheroids formations occurred within 3-7 days post seeding. (**Figure 5,Figure 6,Figure 7**) Spheroid formations were seen with aligned fibers of all diameters (200, 500, 800 nm).

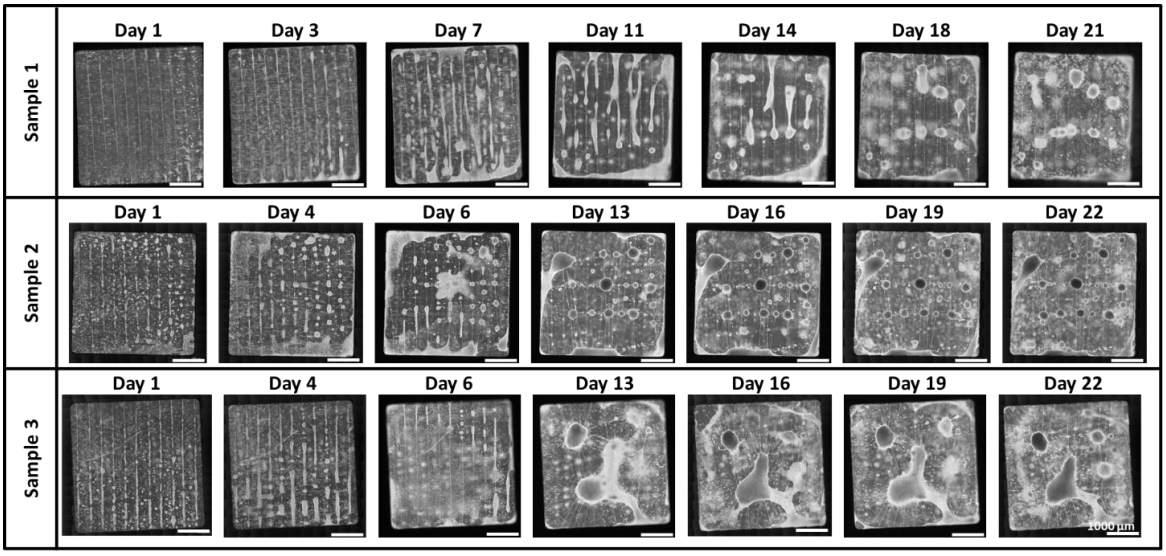

Figure 5: Mosaic images of pericyte cultures on aligned fiber networks with 200 nm aligned fibers and 2 μm base fibers cultured for ~3 weeks (Scale bars: 1000 μm).

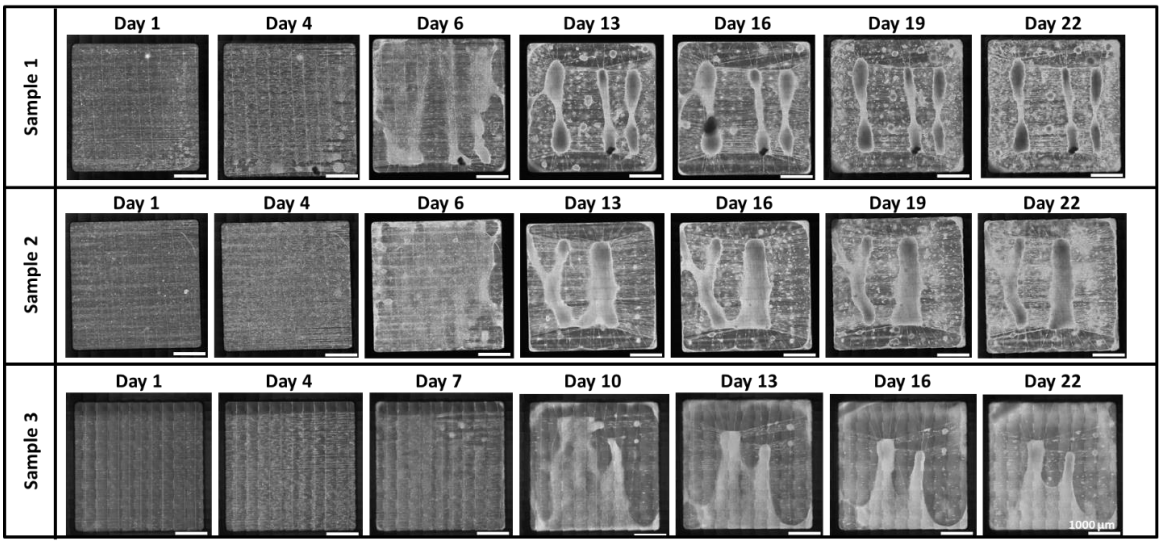

Figure 6: Mosaic images of pericyte cultures on aligned fiber networks with 500 nm aligned fibers and 2 µm base fibers cultured for ~3 weeks (Scale bars: 1000 µm).

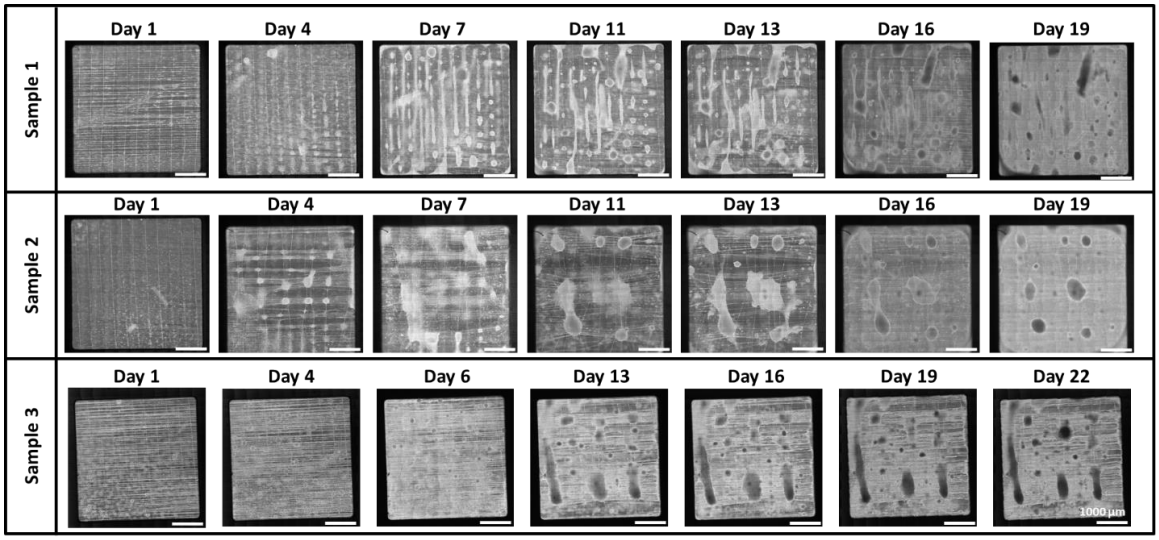

Figure 7: Mosaic images of pericyte cultures on aligned fiber networks with 800 nm aligned fibers and 2 µm base fibers cultured for ~3 weeks (Scale bars: 1000 µm).

These spheroids grew in size and number in the second week of culture. We also noticed cells and spheroids exhibit durotaxis by moving towards the thicker 2 µm orthogonal base fibers, merging with other spheroids in these regions to form long elongated structures (**Figure 8**) around and along the base fibers. On the 200 nm aligned fibers, some of these elongated structures contracted along their major axes forming large individual spheroids over the third week. This process involved marked fiber remodeling

via breaking of the fused junctions. The aligned fibers within the elongated structures were pulled closer together as the structure transformed into spheroids forming networks with other neighboring spheroids (**Figure 9**). Interestingly, with 500 nm aligned fiber networks, most of the cells collectively formed large, elongated structures having large areas and low circularities which persisted through the third week, unlike the 200 nm and 800 nm fiber networks (**Figure 5**,**Figure 6**,**Figure 7**)

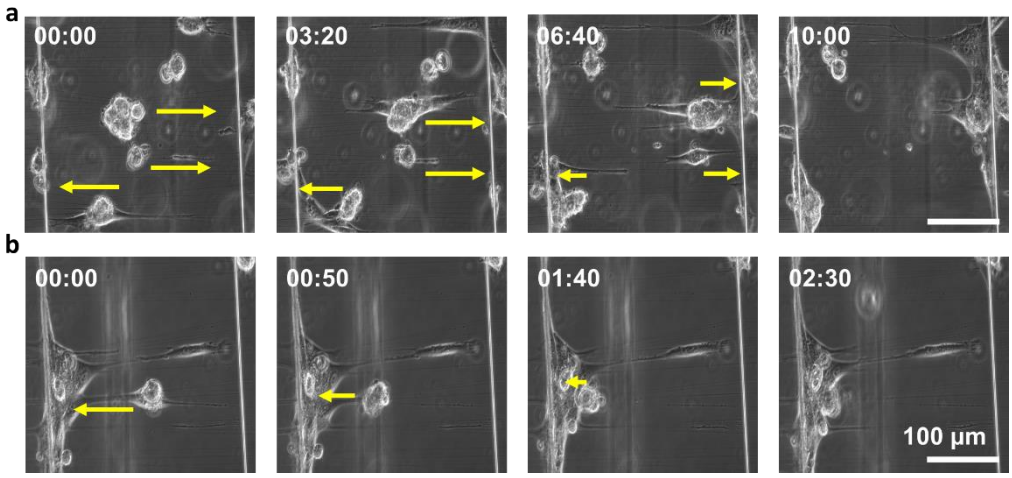

Figure 8: Cells and spheroids (marked in yellow) moving from the aligned fiber regions towards the ~360 µm base fibers (Scale bars: 100 µm, Time stamp: hr:min).

Next, we inquired how these cells reacted to crosshatch fiber networks, which have two orthogonal densely spaced (~10 µm) fibers of the same diameter (either 200, 500 or 800 nm) fused to each other (**Figure 10**,**Figure 11**,**Figure 12**). We found a strong influence of fiber diameter in the crosshatched fiber configuration on the ability of cells to aggregate into spheroids. Among the tested diameters, 200 nm crosshatches were the easiest for pericytes to form spheroids (**Figure 10**). The cells broke the fiber junctions and deformed the fiber networks during spheroid formation. The fibers were aligned almost perpendicular to the spheroid boundaries and formed fiber networks between other spheroids (**Figure 13**). These spheroids exhibited higher circularity throughout their three

weeks in culture, unlike aligned fiber networks, where long structures were predominant at the base fibers during the second week which subsequently contracted into spheroids. Fewer spheroid occurrences were observed on 500 nm crosshatched fiber networks. Regions with spheroids were associated with higher occurrences of fiber remodeling, while cell monolayers were found in intact fibers. (**Figure 11**). On 800 nm crosshatches, pericytes did not form spheroids even after three weeks of culture. Interestingly, pericytes cultured on 800 nm crosshatched networks did not form any spheroids as fiber network integrity was maintained. They preferred to grow as monolayers (**Figure 12**)

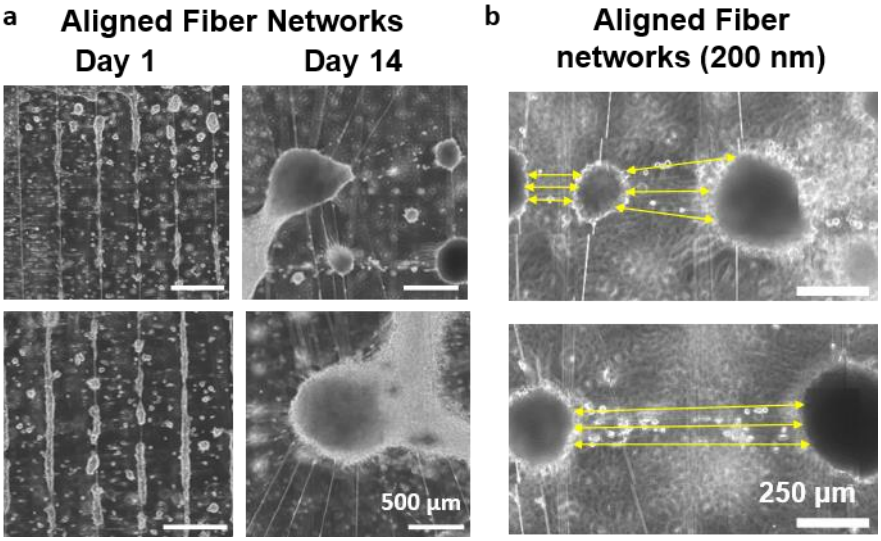

Figure 9: Spheroid formation involve extensive remodeling of the fiber networks in aligned architectures: (a) Day 1 and Day 14 images of the same region of the scaffold after pericytes were seeded on 200 nm aligned fiber networks. (b) Networks of fibers (fibers shown in yellow) formed between spheroids on aligned fiber networks

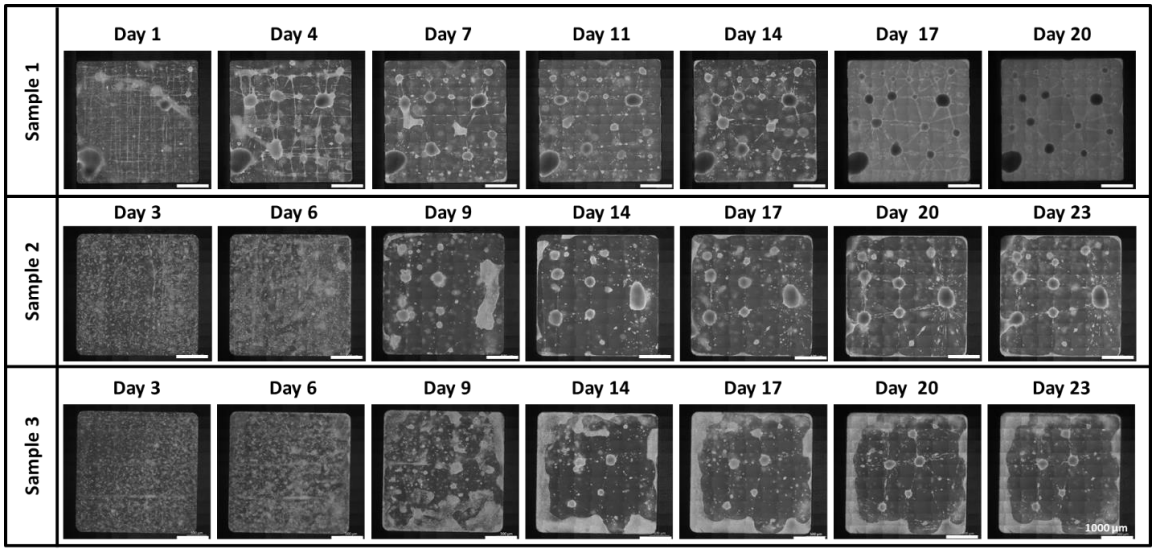

Figure 10: Mosaic images of pericyte cultures on crosshatch fiber networks with 200 nm fibers cultured for ~3 weeks. (Scale bars: 1000 µm).

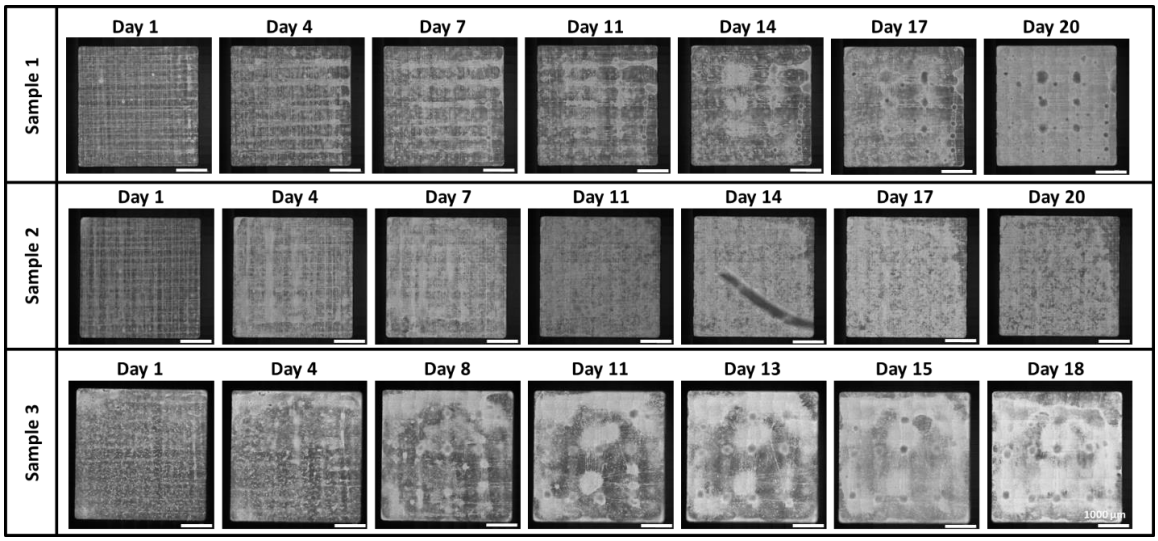

Figure 11: Mosaic images of pericyte cultures on crosshatch fiber networks with 500 nm fibers cultured for ~3 weeks. (Scale bars: 1000 µm).

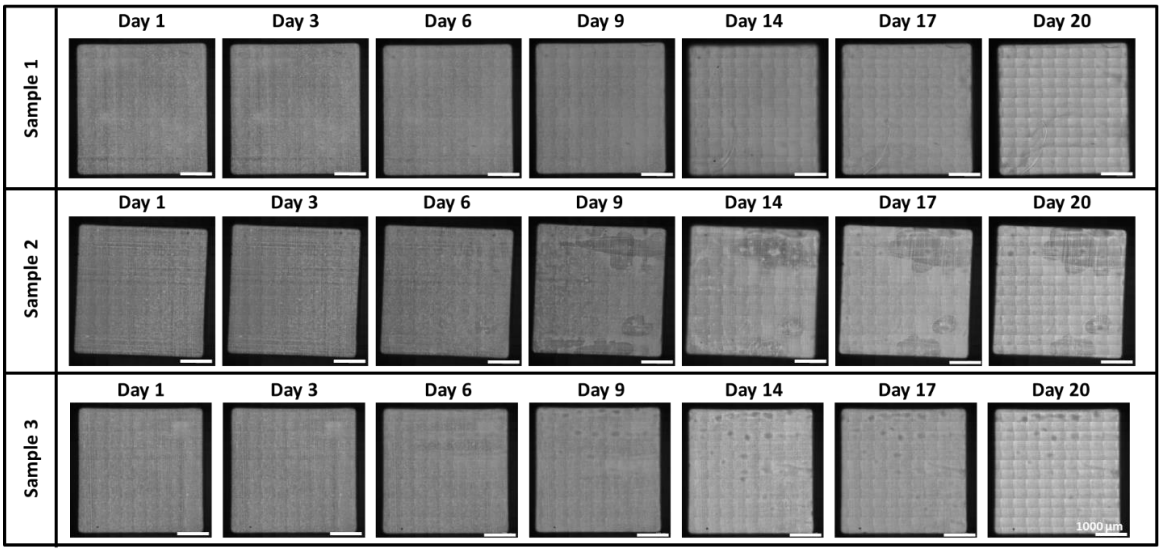

Figure 12: Mosaic images of pericyte cultures on crosshatch fiber networks with 800 nm fibers cultured for ~3 weeks. (Scale bars: 1000 µm).

With precise control over fiber architecture and diameter, we explored the extent of biophysical influence of the underlying fiber architecture to direct pericyte aggregation. We designed fiber networks with monolayer-forming 800 nm crosshatch regions interspaced with spheroid-forming aligned 200 nm diameter fiber networks and hypothesized that these scaffolds would result in a mix of monolayers and spheroids. Indeed, spheroid formations were only seen on aligned fiber regions while monolayers were seen on crosshatched regions, providing a novel method to have spatial control over cell aggregation (**Figure 14**).

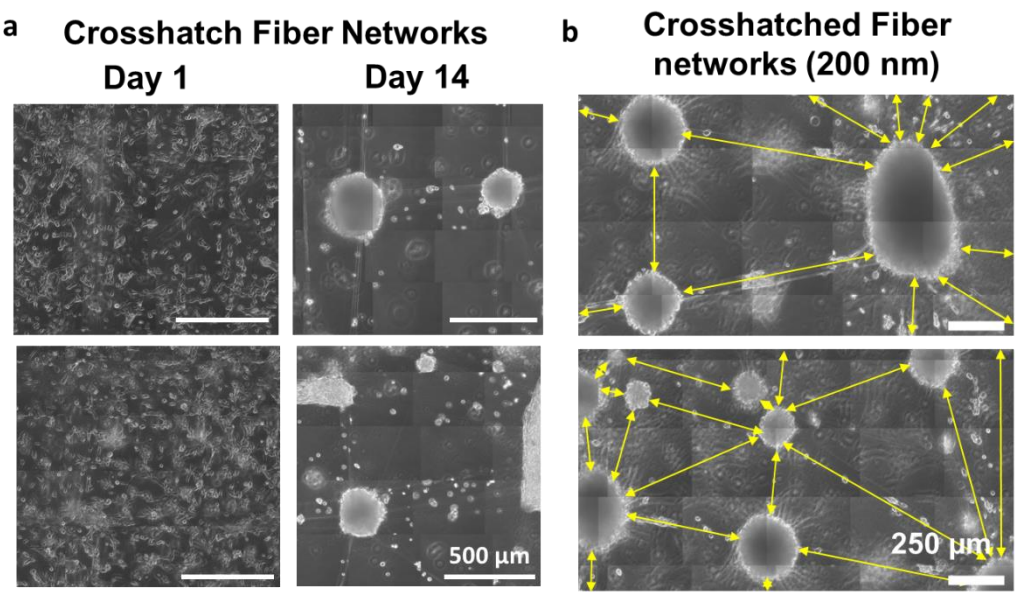

Figure 13: Spheroid formation involve extensive remodeling of the fiber networks in crosshatched architectures: (a) Day 1 and Day 14 images of the same region of the scaffold after pericytes were seeded on 200 nm crosshatched fiber networks. (b) Networks of fibers (fibers shown in yellow) formed between spheroids on crosshatched fiber networks

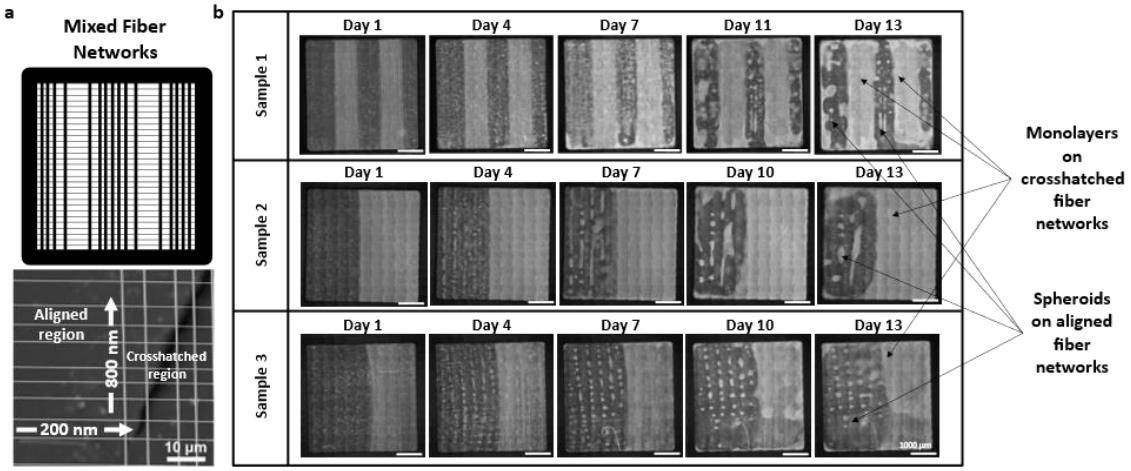

Figure 14: (a) Representative image (top) and a SEM image of a zoomed in section (bottom) of a mixed fiber network with aligned regions of 200 nm aligned fibers and 800 nm base fibers and crosshatch regions with 200 nm and 800 nm fibers deposited. Scale bar: 10 µm. (b) Mosaic images of pericyte cultures on mixed fiber networks with cultured for ~2 weeks. (Scale bars: 1000 µm).

From the mosaic images of the fiber networks taken every 2-4 days, we quantified various metrics to better understand spheroid growth and culture on fiber networks. On 200 nm aligned fiber networks we observed cellular aggregates of large areas (0.15±0.04 mm^2) and low circularities (0.37±0.02) on the base fibers (**Figure 15**) and were similar to 800 nm aligned fiber networks. These elongated structures contracted in the third week of culture and had a more spherical morphology (**Figure 15**). The trends on 200 nm and 800

nm aligned fiber networks were similar. However, with 500 nm aligned fiber networks, we observed elongated structures of extremely large areas (2.29±1.67 mm^2) and low circularities (0.34±0.18) that persisted from the second week of culture (**Figure 15**). With crosshatches, 200 nm fibers had higher number of spheroid occurrences throughout the three weeks of culture, while the circularities and areas of the spheroids for both fiber diameters showed similar trends (**Figure 15**).

Thus, we developed spatial control over pericyte aggregation using biophysical cues from control over the underlying fiber matrix.

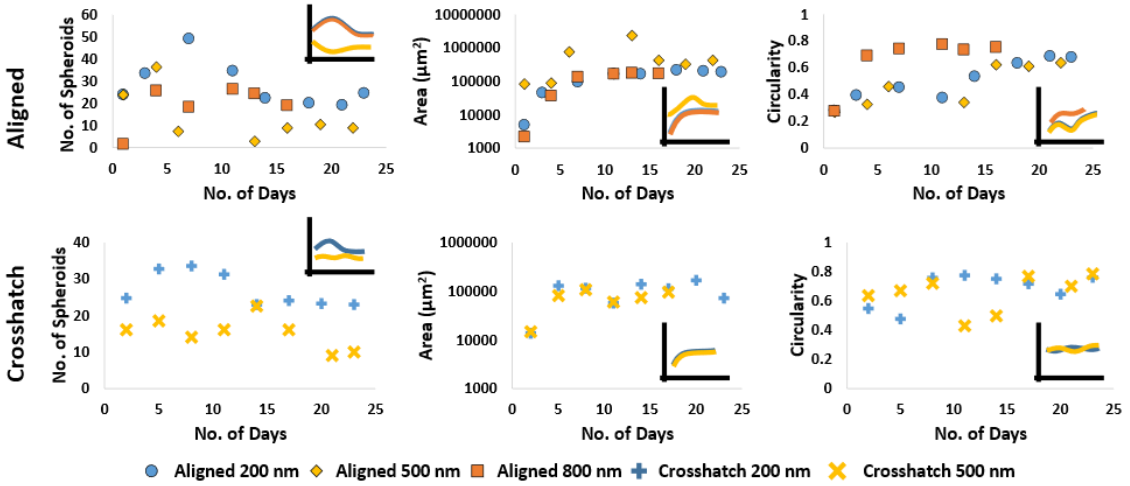

Figure 15: Changes in the number, area, and circularity of spheroids with time when cultured on suspended fibers of varying diameter (200, 500 & 800 nm) and architecture (aligned and crosshatch).

2.3 Spheroids exhibit dynamic interactions with their surrounding microenvironment

Next, we inquired how spheroids dynamically interacted with their surrounding microenvironment, namely individual pericytes, other spheroids using the fiber networks from timelapse imaging over short intervals (~8-24 hours). On 200 nm aligned fiber networks, multiple occasions of spheroids exhibiting durotaxis by moving along the aligned fibers towards the stiffer base fibers were seen (**Figure 8**, **Figure 16**). In certain instances, spheroids were observed to be pulled by single or few cells (**Figure 17b**),

while in other cases, the cells responsible for pulling the spheroids were not visible (**Figure 17a**). Once on the larger diameters, the spheroids were observed to grow in size and generally not move back to the smaller diameter fibers. We tracked the migration speeds and persistence (ability to move in the same direction) of the spheroids and individual cells. Spheroids migrated either as a whole (velocity: 42.24±16.47 μm/hr, persistence: 0.65± 0.19, n=8, **Figure 17c,d**) or by being pulled by an individual cell (velocity: 33.82±10.04 μm/hr, persistence: 0.69± 0.21, n=13, **Figure 17c,d**) and were seen to be slower and less persistent than cells (velocity: 46.52±19.64 μm/hr, persistence: 0.78± 0.32, n=23, **Figure 17c,d**).

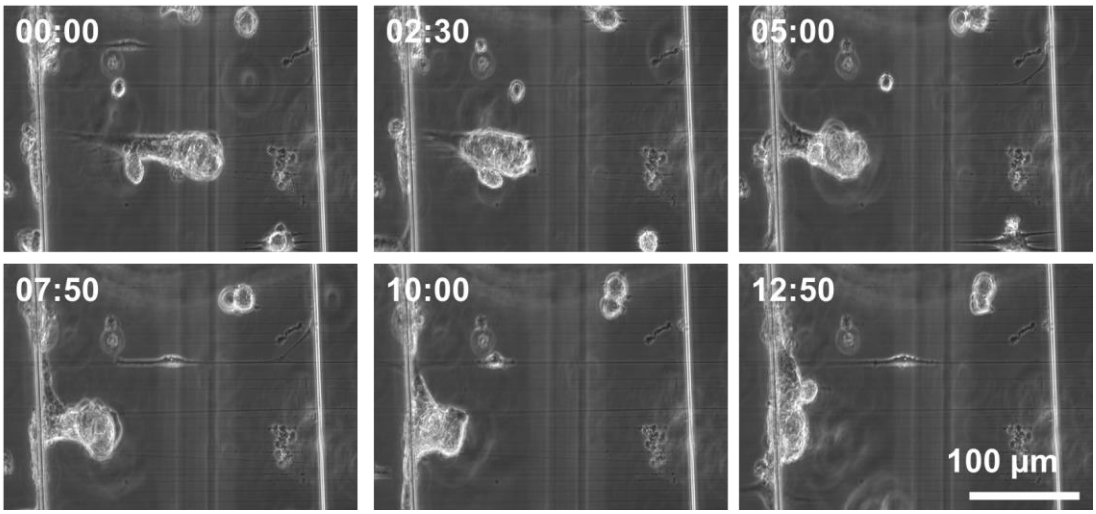

Figure 16: A spheroid moving towards a base fiber (Scale Bar: 100 μm, Time stamp: hr:min)

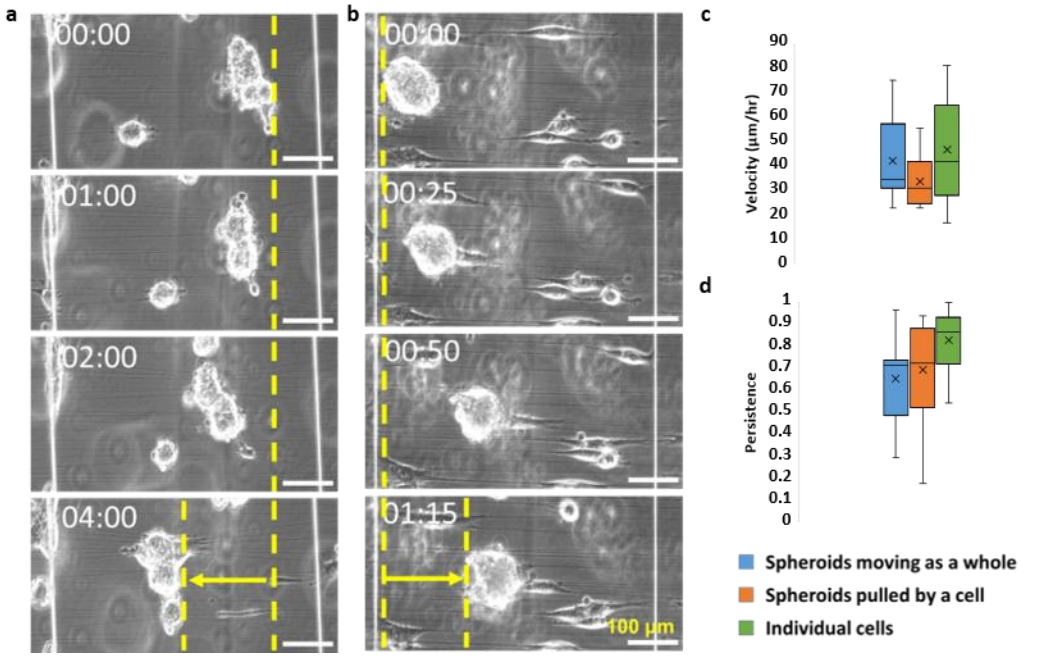

Figure 17: (a) Time lapse images of spheroids migrating along aligned fibers (a) as a whole and (b) while being pulled by a cell (Scale Bar: 100 µm) (c) Average velocity (µm/hr) and (d) persistence of spheroids being pulled by a cell (N=13), spheroids moving as a whole (N=8) when compared to individual cell migration (N=23).

Individual cells were seen sprouting and moving away from spheroids or migrating towards and joining spheroids (**Figure 18a**), facilitated by fiber connections into the spheroids. Tracking the outward (efflux) and inward (influx) movement of cells from random spheroids at different locations and in culture for 7-14 days, we observed that the average cumulative efflux out of the spheroid after 24 hours (25.28±3.3) was higher (p=.01) than the average cumulative influx into the spheroid (14.17±2.24) (**Figure 18b**). We calculated the net outward cell movement, which is the cumulative difference between the cells migrating away and those migrating into the spheroid and found that when the net outward cell movement rapidly increased, the spheroid area remained constant. We also found the cell movement rate decreased gradually which was concomitant with an area increase (**Figure 18c**). The net outward cell flow rate of the spheroids was independent of the area of the spheroid **Figure 18d**).

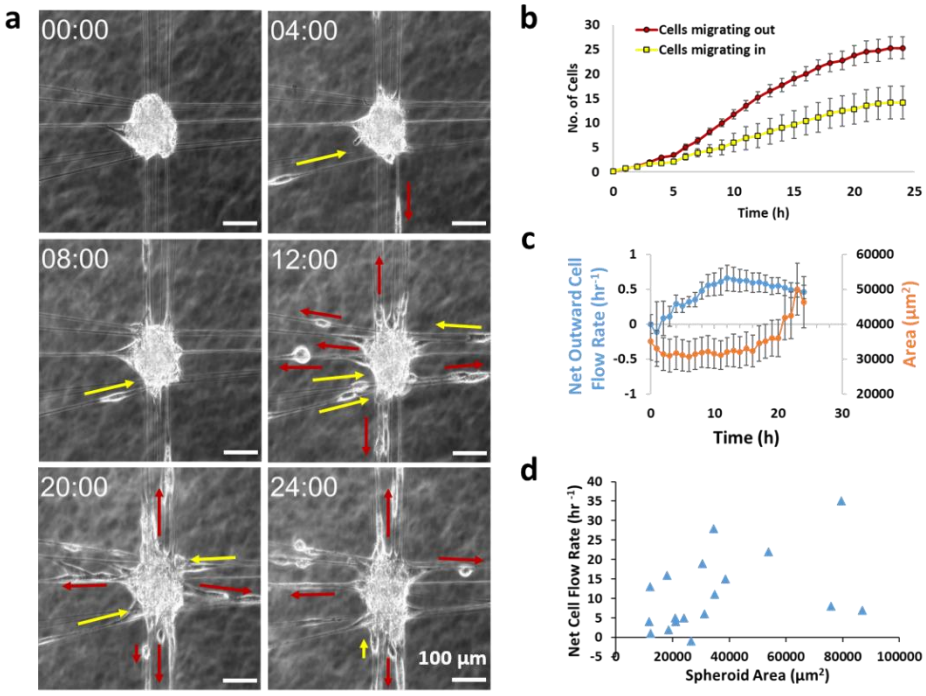

Figure 18: (a) (i)Time lapse images of cells continuously moving into (blue arrows) and moving out of (red arrows) individual spheroids. (Scale Bar: 100 µm) (b) Cells migrating out of spheroids occurred with a higher frequency than cells migrating into the spheroid over time (N=18, error bars represent standard error). (c) Changes in outward cell flow rate and area with time in spheroids when cells are moving into and out of these spheroids (N=18, error bars represent standard error) (d) Net outward cell flow rate was independent of area when cells were migrating into and moving out of spheroids. (n=18).

On both aligned and crosshatch fiber networks, we show extensive remodeling of the fibers during spheroid formation and culture and spheroids interacted with other spheroids at different locations in the fiber networks via fibers by exchanging cells between them (**Figure 9**, **Figure 13**). Spheroid mergers (

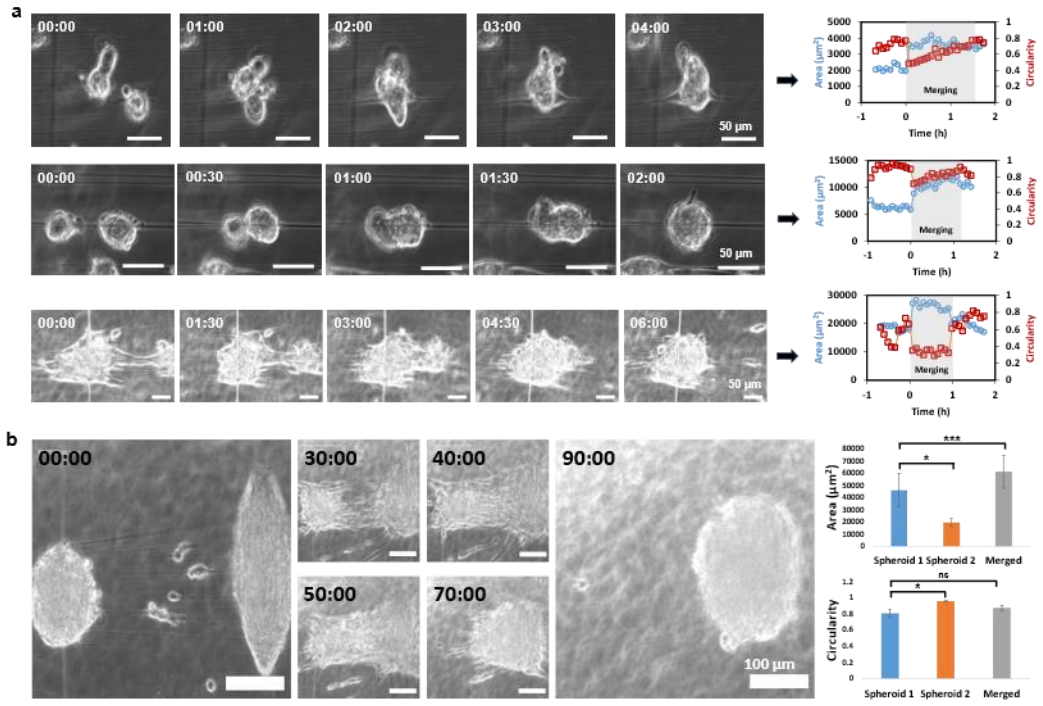

Figure 19a) were also a common way of increasing their size. On aligned fiber networks, multiple cells and spheroids accumulated and merged at the base fibers and formed elongated structures. These large, elongated structures and large spheroids exhibited a combination of all the previously mentioned interactions simultaneously and involved extensive fiber deformations including deformations of the stiff base fibers indicative of extremely large forces (**Figure 9**, **Figure 13**).

We also observed multiple instances on aligned fiber networks where two spheroids with a large difference in area merge into each other without migrating (

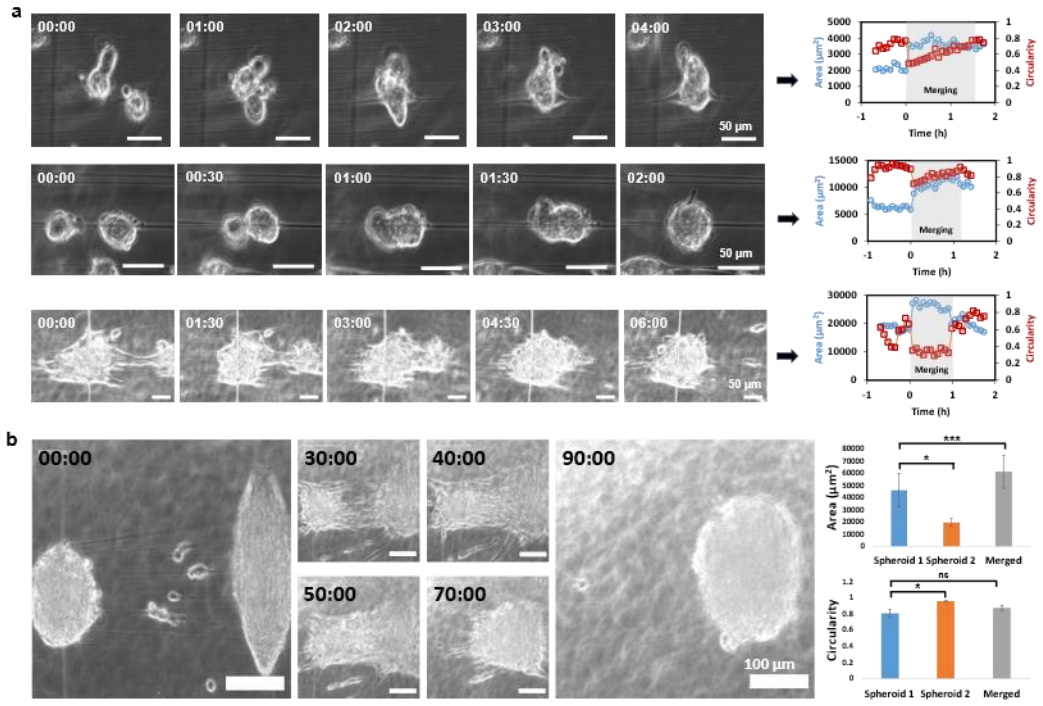

Figure 19b). In such instances, cells were initially seen traveling between these spheroids via fibers, with the number of cells increasing over time to form a bridge of cells filling the gap between the spheroids. The combined structure then contracted inwards and their spherical shape was regained. Data showed the area of the merged spheroid increased significantly while the circularity was maintained after merging.

Overall, we demonstrate unique multiple cell-spheroid, spheroid-spheroid, and spheroid-fiber interactions that either led to their migration, increase in size or change in shape.

2.4 Forces & contractility in spheroids

Since pericyte aggregation deflected the fibers, we quantified the contractile forces involved during their aggregation. Using our established nanonet force microscopy technique[50–53,56] , we calculated the transient contractile forces exerted from the point

when multiple individual cells came into contact with each other until they assembled into spheroids. As the collective area occupied by the cells decreased due to formation of spheroids, the average forces reduced from 1294±466 nN during the start of formation to 301±368 nN when spheroids were fully formed (n=16) while area reduced from 14,778±2614 μm^2 to 8012±947 μm^2 (p=.02, n=18) (**Figure 20a**). Spheroids exerted significantly higher forces (p<.001) when compared to individual pericytes. Individual cells had an average force of (48.71 ± 27.03 nN, n=23), while spheroids had a wide range of forces (1472 ± 1810 nN, N=46) depending on their area. Spheroid forces increased with increase in area (**Figure 20b**, n=49). We found that cells sprouting (exiting) the spheroids led to a decrease in forces by ~45% from 1564 ± 1849 nN to 1027 ± 1619 nN (p=0.2, n=21), while the area reduced by an average of 14% from 6993 ± 2473 μm^2 to 6041 ± 1721 μm^2 (p=.006, n=21, **Figure 20c**).

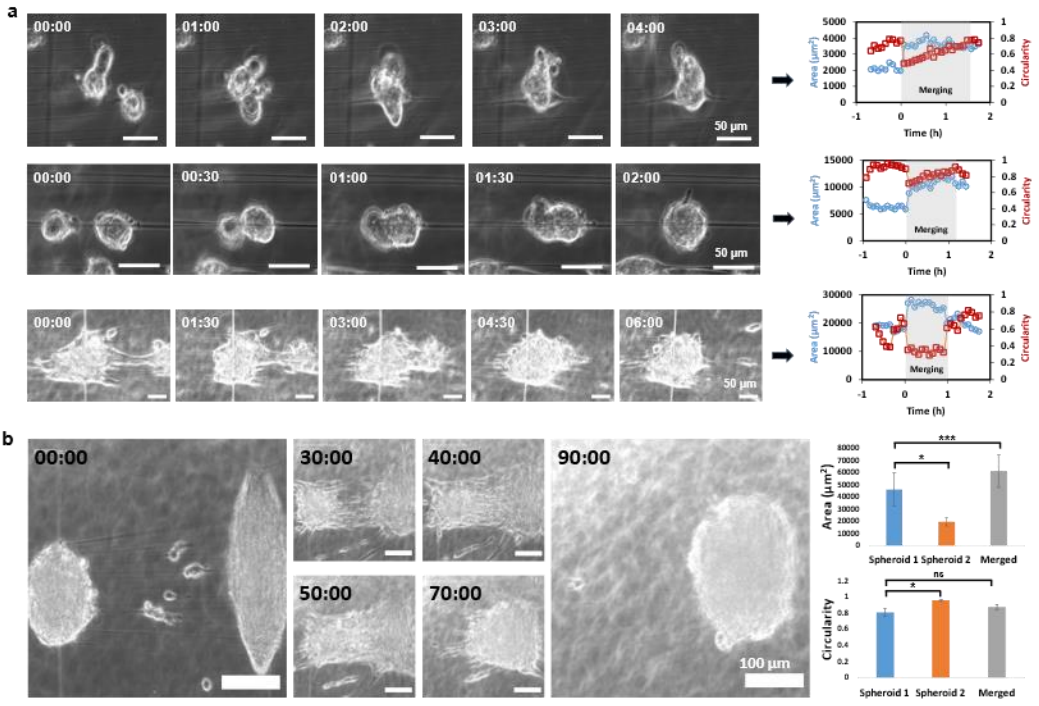

Figure 19: (a) Time lapse images of different instances of two spheroids merging with each other. The graphs on the right show the changes in area and circularity in the larger spheroid when another spheroid merges into it. Scale bars: 50 µm, Time Stamp: hr:min (b) Time lapse images (left) of two large spheroids merging via initial exchange of cells leading to a bridge of cells between the two spheroids followed by merging into a large spheroid. The graphs (right) show the changes in area and circularity of the individual spheroids before and after merging (N=15). Scale bars: 100 µm,Time Stamps: hr:min

To further study the role of contractility, we perturbed the spheroid contractility by inhibiting ROCK using Y-27632 (**Figure 21**). We observed that spheroids rapidly (within 1-2 hrs.) lost their compactness and cells migrated away along the aligned fibers without apparent loss of cell-cell adhesion (**Figure 21a**), as evidenced by an increase in the area and a decrease in the circularity (**Figure 21b**). Addition of Y-27632 reduced the force per unit area exerted on fibers by the spheroids significantly (P=.02) from 2.66 nN/µm^2 to 0.73 nN/µm^2 (n=10) (**Figure 21b**). The impact of ROCK inhibition was reversible.

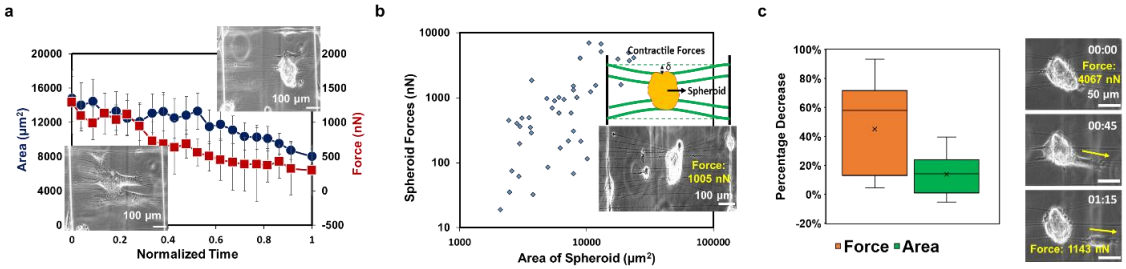

Restoring control conditions by washing off the drug and replacing the culture media after 4 hours caused the cells to quickly reform spheroids after 6-8 hours and regain pre-drug state (**Figure 21a,b**). Increasing the dose from 10 µM to 20 µM and treatment time from 4 hours to 8 hours and 15 hours produced similar effects (Error! Reference source n ot found.). ROCK inhibition prior to spheroid formation prevented 3D aggregation and caused the pericytes to grow into monolayers (**Figure 23**). Reversal by drug wash off showed cells immediately contracting towards each other at multiple locations to form spheroids and elongated structures within 24 hours as seen in the control culture.

Figure 20: (a) Clusters of cells (inset, left) undergo dynamic changes in contractile forces (N=16) and area (N=18) during formation of a spheroid (inset, right) (Error bars: Standard error, Inset scale bars: 100 µm). (b) Spheroid forces

with respect to area of the spheroid (N=49). Inset: A representative image of fibers being deflected by spheroids (top) and a pericyte spheroid (bottom) deflecting the aligned fibers by exerting contractile forces (Scale bar: 100 µm). The displacement of the fibers is converted to forces through the stiffness of the fibers modelled as fixed-fixed beams. (c) Percentage decrease in contractile forces and area of spheroids after an individual cell sprouts out of the spheroid (N=17) Inset images show an individual cell (marked in yellow) sprouting out of a spheroid (Scale bar: 50 µm, Time stamps: hr:min).

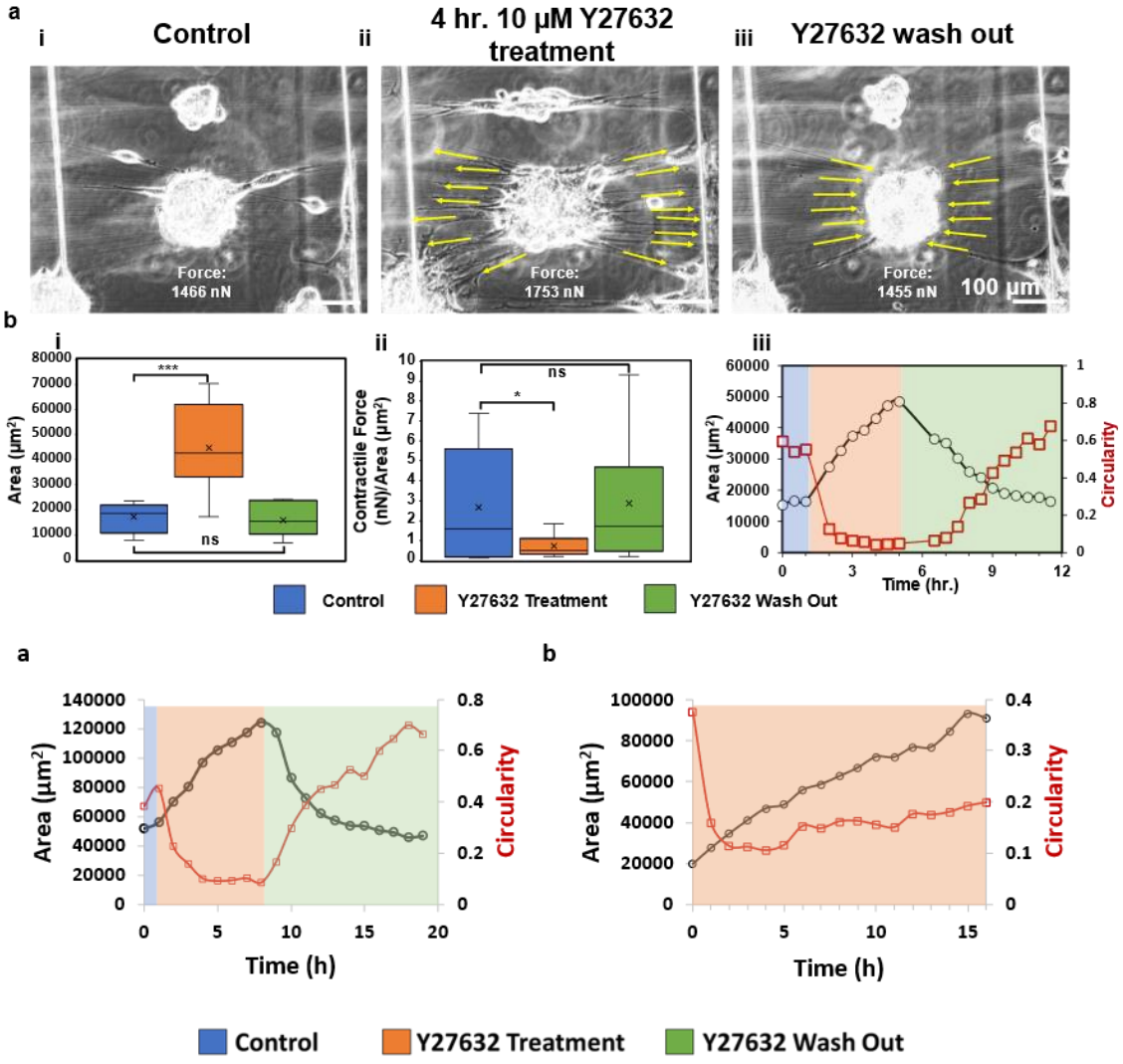

Figure 21: (a)(i) Effect of treatment of 10 µM Y-27632 (ROCK-inhibitor) for 4 hours on spheroids. Cells within the spheroids lose their contractility and are seen coming out of the spheroid (indicated by yellow arrows) (iii) Recovery of the spheroids after drug wash off. The cells regain contractility and move back into the spheroid by 12 hours (Scale bars: 100 µm). (b) Changes in (i) area and (ii) contractile forces per unit area during Y-27632 treatment and after Y-27632 wash out (N=10). (iii) Dynamic changes in area and circularity of the spheroids during Y-27632 treatment and after Y-27632 wash out (N=10)

Figure 22: (a) Area and circularity changes in spheroids under control conditions, when treated with 20 µM Y-27632 for 8 hours, and after Y-27632 was washed off (N=6). (b) Area and circularity changes in spheroids when treated with 20 µM Y-27632 for 15 hours (N=13).

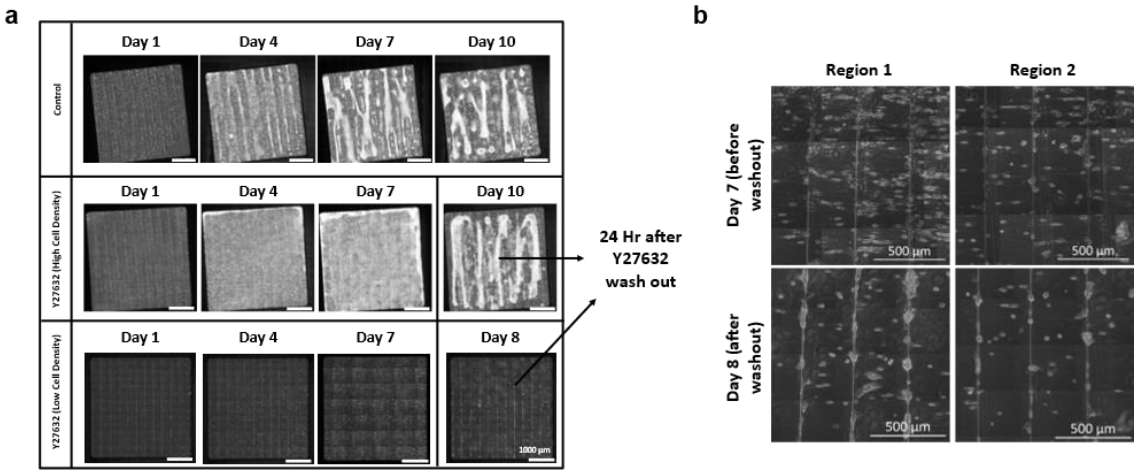

Figure 23: (a) Growth of control pericyte cultures compared to pericyte cultures seeded with 20 µM Y-27632 in the media. 24 hours after drug wash out shows similar structures as seen in control cultures. Cells grew into monolayers if the cell density was high or did not form spheroids with lower cell densities when treated with Y-27632 from Day 01 to Day 07. Elongated aggregates along the base fibers and spheroids were seen after reversal with high cell density while small spheroids formed after reversal when the cell density was low. (b) Zoomed in images of the low cell density scaffold treated with Y-27632 showing clusters of cells turning into spheroids after Y-27632 wash out.

Next, we inquired if changes in gene expression are associated with dynamics of spheroid formation. From RNA isolated from spheroids on 200 nm aligned fiber networks on days 1, 7, 14, and 21, we compared contractility markers *Acta2*, *Cnn1*, *Sm22*, and *Smtn* (**Figure 24**). No significant changes were seen with the gene expressions on day-1 post-seeding when placed on fiber networks compared to 2D monolayer culture (P=.059). However, *Acta2* expression decreased between day 7 and day 14 on fiber networks (0.060 ± 0.015 vs 0.015 ± 0.004, P=.045). *Cnn1* expression was downregulated, approaching close to statistical significance on both day 7 and day 14 when compared with day one (0.011 ± 0.004 vs 0.002 ± 0.001, P=.056 and 0.011 ± 0.004 vs 0.001 ± 0.001, P=.051, respectively); however, these differences did not reach statistical significance within 5% confidence. *Sm22* expression displayed a clear decrease with time on fiber networks compared to the first day of seeding on the scaffolds (day 14: day 1→0.076 ± 0.002 vs 0.363 ± 0.042, P=.002 and day 21: day 1→ 0.026 ± 0.010 vs 0.363 ± 0.042, P=.001, respectively). By 21 days post seeding, *Smtn* gene expression was

significantly decreased compared to day 1 gene expression (0.025 ± 0.002 vs 0.094 ± 0.022, P=.036). Additionally, day 7 and day 14 showed a trend for decreasing *Smtn* gene expression compared to day 1 (0.039 ± 0.012 vs 0.094 ± 0.022, P=.092 and 0.027 ± 0.011 vs 0.094 ± 0.022, P=.054), which did not reach statistical significance within 5% confidence.

Overall, we report the change in forces as spheroids are formed and the role of contractility in maintaining their structure.

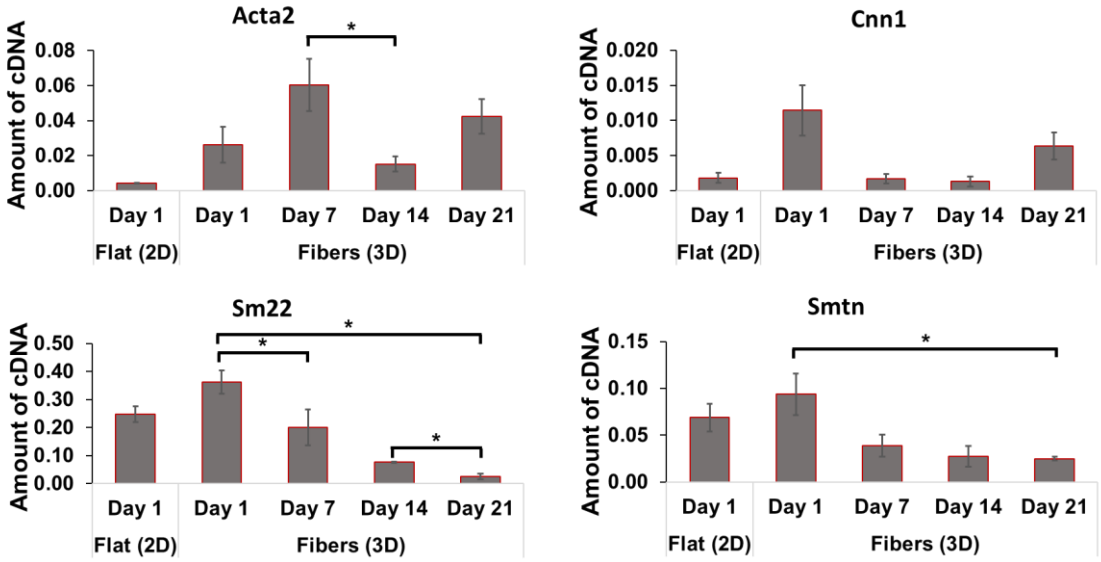

Figure 24: *Acta2*, *Cnn1*, *Sm22*, and *Smtn* gene expressions in pericytes cultured on either 2D plates (collected on Day 1) or on fiber networks (collected on Day 1, Day 7, Day 14, and Day 21 post-seeding).

2.5 Pulsing in Spheroids

After ~2 weeks in culture, we observed pericyte spheroids pulsing at regular time intervals. The spheroids were observed to beat, with their area increasing and decreasing at an average frequency of 4.5 ± 0.75 beats/hour and an average pulse width (or the change in area during a pulse) of 2108.27 ± 846.68 μm^2 (n=14) (**Figure 25**). We tracked the pulsing of these spheroids for 20 hours to observe how their frequency and pulse width change with time. We found that over 20 hours, their frequency increases from 4.46 ± 0.69 beats/hour to 4.57 ± 0.72 beats/hour while their pulse width decreased from 2167.02 ± 936.05 μm^2 to 2057.59 ± 689.18 μm^2, which implies that the pulses are getting faster but with a smaller change in area. The spheroids also decreased in area between after 12 hours from 47010.79 ± 17845.96 μm^2 to 44307.91 ± 15136.56 μm^2 while their circularity increased from 0.81 ± 0.11 to 0.5 ± 0.09, and subsequently increased in area back to 47307.89 ± 15863.85 μm^2 with the circularity unchanged at 0.86 ± 0.10 after 18 hours. Thus, the spheroids are very dynamic in nature, and are constantly beating while having other interactions as discussed in previous sections and their ability to contract plays a key role in this behavior.

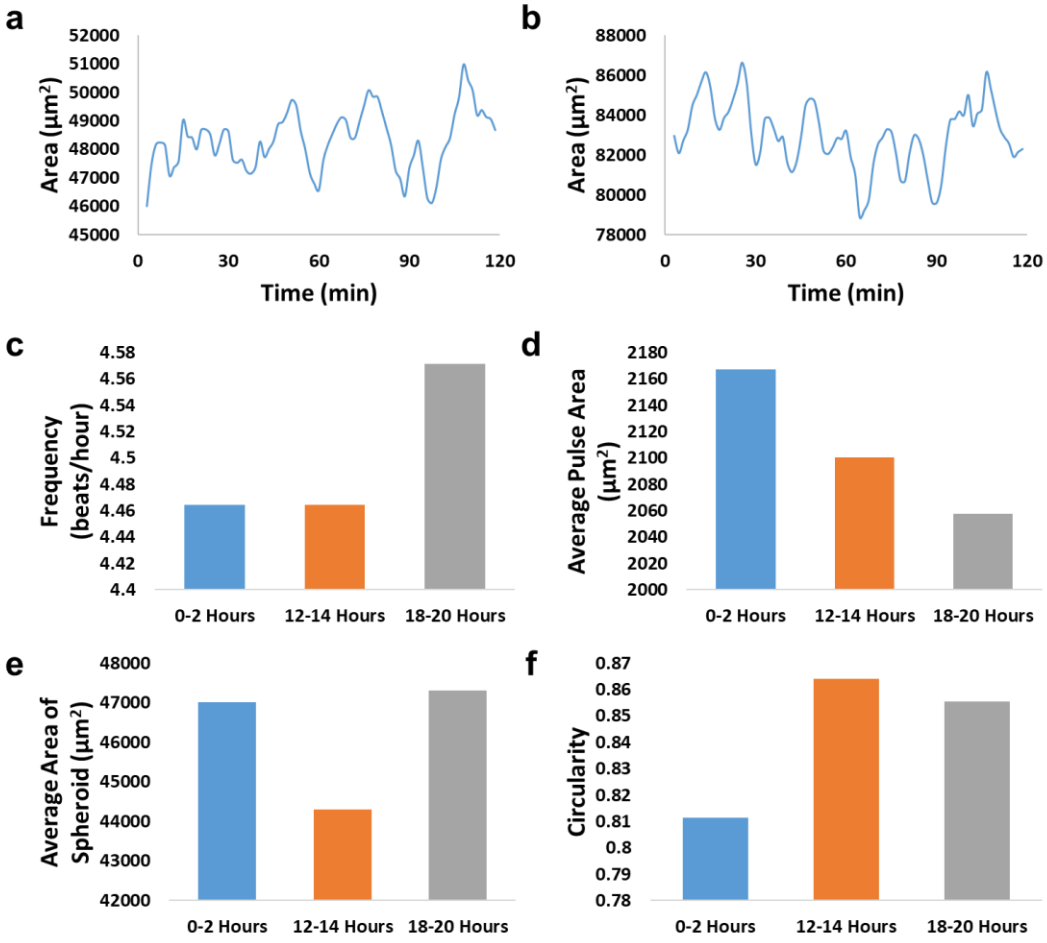

Figure 25: (a, b) Changes in area over time as two spheroids pulse with time. Changes in (c) average frequency, (d) average pulse width, (e) average area, and (f) average circularity of the spheroid over 20 hours. (n=14)

2.6 Effect of seeding density

The number of cells available for spheroid formation would depend on the initial seeding density of the cultures. Thus, we wanted to enquire how the seeding density influences spheroid formation. We seeded pericytes with varying cell densities (300k, 440k, 1200k, and 4000k cells/mL) on crosshatched fiber networks of different fiber diameters (200, 500 and 800 nm) and tracked them for three weeks. We found that a low seeding density (300k cell/mL) had too few cells for spheroid formation and a lot of empty spaces were seen in the fiber networks even after three weeks of culture with the fiber networks

mostly intact. Some spheroid-like structures were seen in 200 nm crosshatched networks in the third week (**Figure 26**). With 440k cells/mL, spheroid formations were the maximum compared to other seeding densities. Both 200 and 800 nm fiber networks produced spheroids and aggregated structures (**Figure 27**). With higher seeding densities (1200k and 4000k cells/mL), cultures formed dense monolayers by the end of three weeks (**Figure 28, Figure 29**). Initially, in 200 nm crosshatched fiber networks (within the first week), multiple spheroids were seen at various locations but with time, these merged together into monolayers (**Figure 28,Figure 29**). Thus, ideal seeding densities would be greater than 300k cells/mL but lower than 1200k cells/mL.

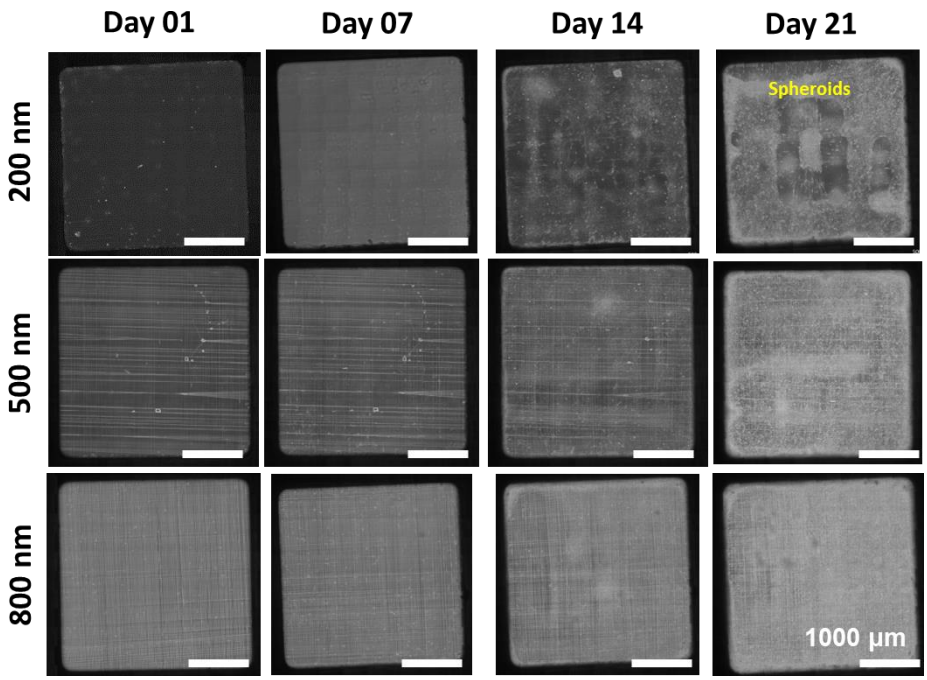

Figure 26: Mosaic images of pericytes seeded on 200, 500 and 800 nm crosshatch fibers with a seeding density of 300,000 cells/mL and imaged every week for three weeks (Scale bar: 1000 µm)

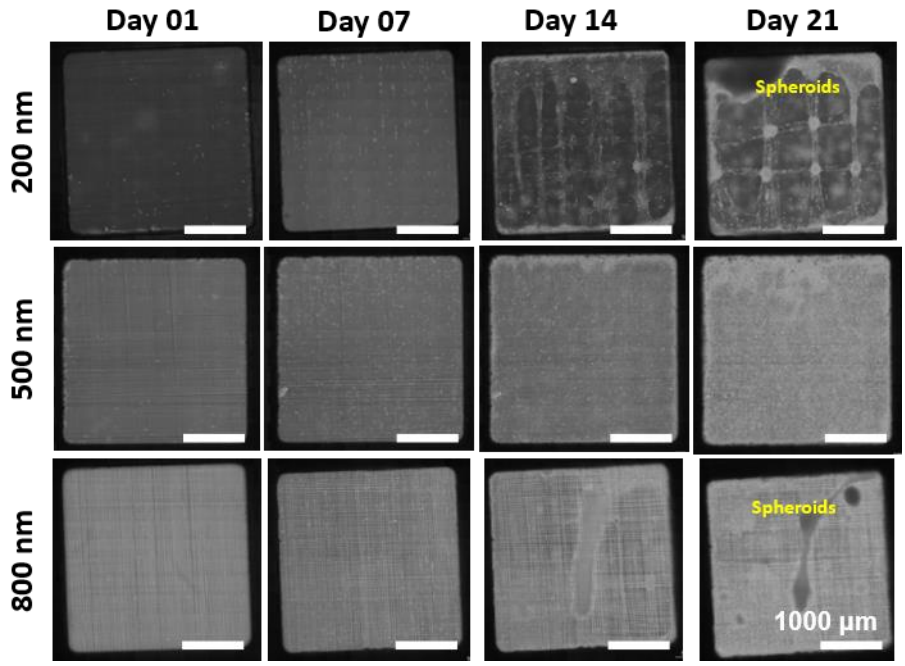

Figure 27: Mosaic images of pericytes seeded on 200, 500 and 800 nm crosshatch fibers with a seeding density of 440,000 cells/mL and imaged every week for three weeks (Scale bar: 1000 µm). Spheroids were seen on 200 nm and 800 nm crosshatches.

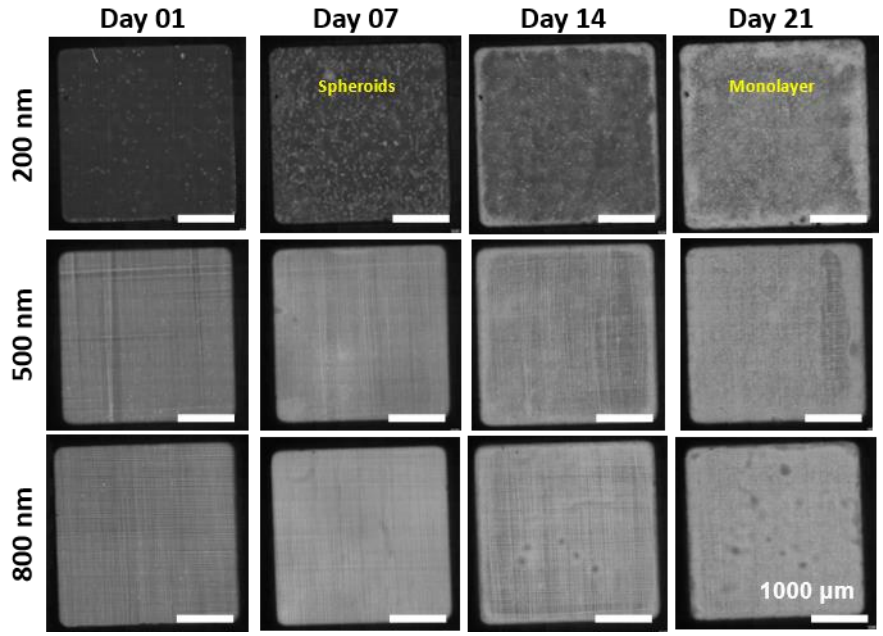

Figure 28: Mosaic images of pericytes seeded on 200, 500 and 800 nm crosshatch fibers with a seeding density of 1,200,000 cells/mL and imaged every week for three weeks (Scale bar: 1000 µm). Small spheroids were seen initially on 200 nm crosshatches which later turned to monolayers (indicated in yellow).

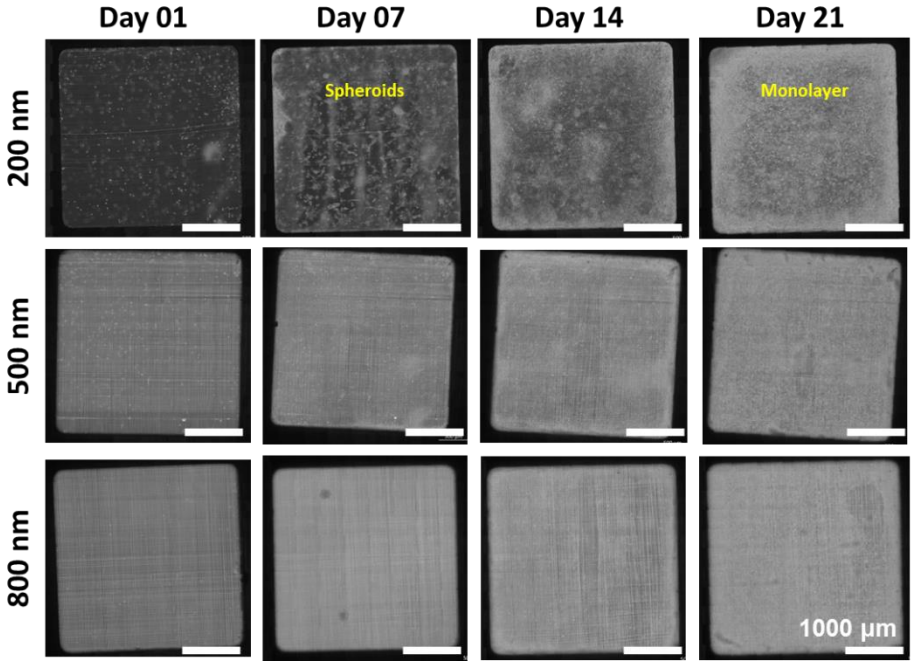

Figure 29: Mosaic images of pericytes seeded on 200, 500 and 800 nm crosshatch fibers with a seeding density of 4,000,000 cells/mL and imaged every week for three weeks (Scale bar: 1000 µm). Small spheroids were seen initially on 200 nm crosshatches which later turned to monolayers (indicated in yellow).

2.7 Geometric design changes with fiber networks lead to variations in spatial organization of the spheroids

To understand how the spacing between fibers influences spheroid cultures, we cultured pericytes on new fiber architectures as shown in **Figure 30** with increased inter fiber spacing in the vertical direction. In the fiber network shown in **Figure 30a**, we increased the spacing of the base fibers from 360 μm to 500 μm of the 800 nm aligned fibers. We saw very similar behavior of pericyte spheroid and aggregate formation to our 800 nm aligned fiber networks (**Figure 7** vs **Figure 31**). We then seeded pericytes on fiber networks as shown in **Figure 30b** where the 200 nm fibers are predominantly in the horizontal direction with the same spacing as in the aligned direction. These fiber networks are similar to the 200 nm aligned fiber networks but without the base fibers in the vertical direction except the central base fiber, implying an extremely large inter fiber spacing in the vertical direction. We saw spheroids forming in the aligned regions of these fiber networks as well (**Figure 32**). Large spheroids were seen in the central base fiber which is in the vertical direction. We also tried a third fiber network **Figure 30c**, where the 2 μm base fibers of the aligned fiber networks are replaced with 200 nm fibers. With these networks, we saw very similar behavior in terms of spheroid formation and growth when compared to the 200 nm aligned fiber networks (**Figure 5** vs **Figure 33**). These results would suggest that in aligned fiber networks, these cells will form similar structures regardless of the base fiber diameter and the spacing between the fibers in the vertical direction and indicate that fiber orientation equally impacts cell aggregation.

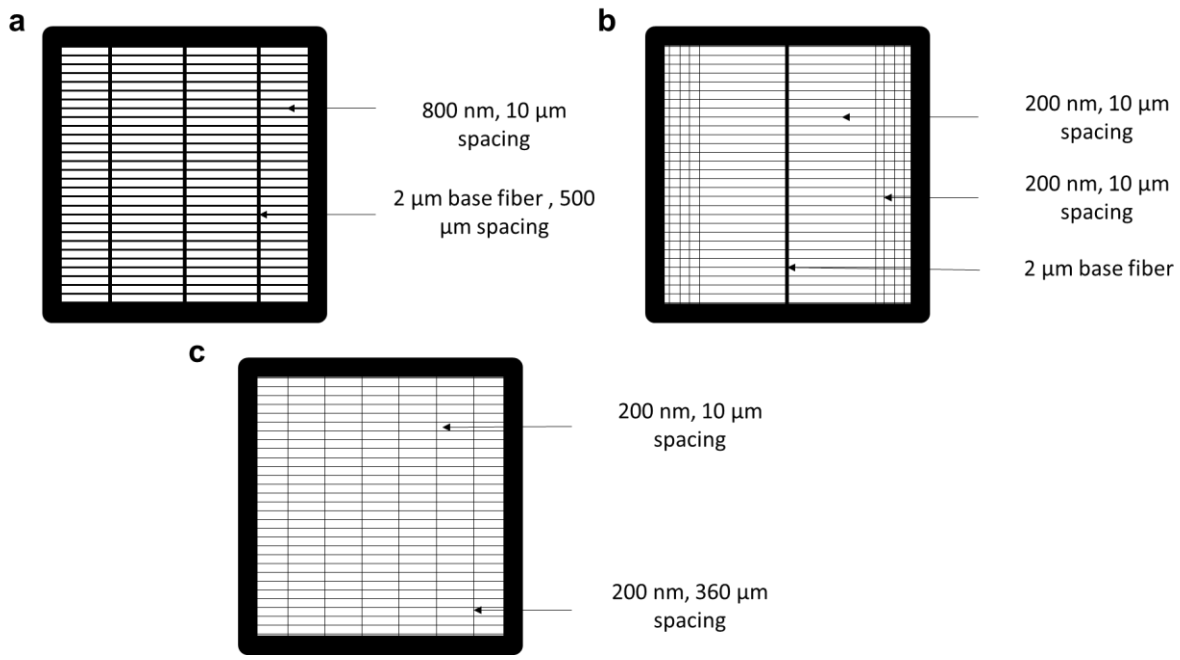

Figure 30: (a) 800 nm aligned fiber networks with wide (500 µm) spacing between the base fibers. (b) Fiber networks with 200 nm aligned regions in the horizontal direction and just one 2 µm base fiber at the center in the vertical direction. The 200 nm fibers in the vertical direction near the ends help in maintaining the integrity of the scaffolds during seeding. (c) 200 nm aligned fiber networks with 200 nm fibers in the vertical direction.

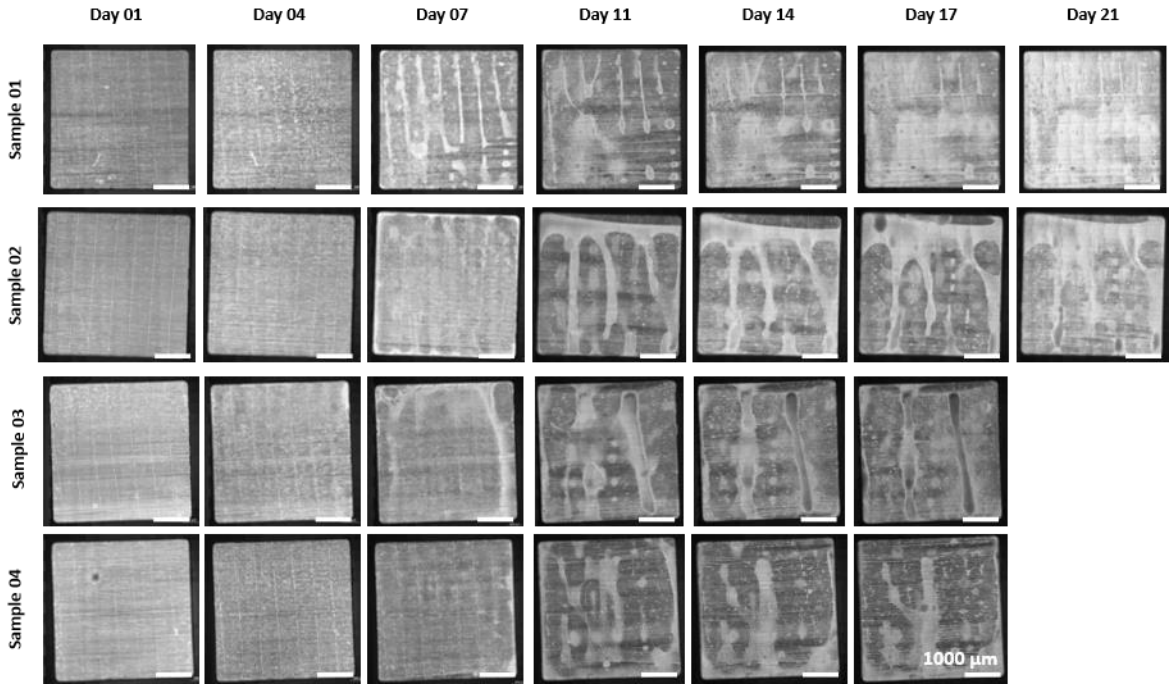

Figure 31: Mosaic images of pericytes seeded on widely (500 µm) spaced 800 nm aligned fiber networks.

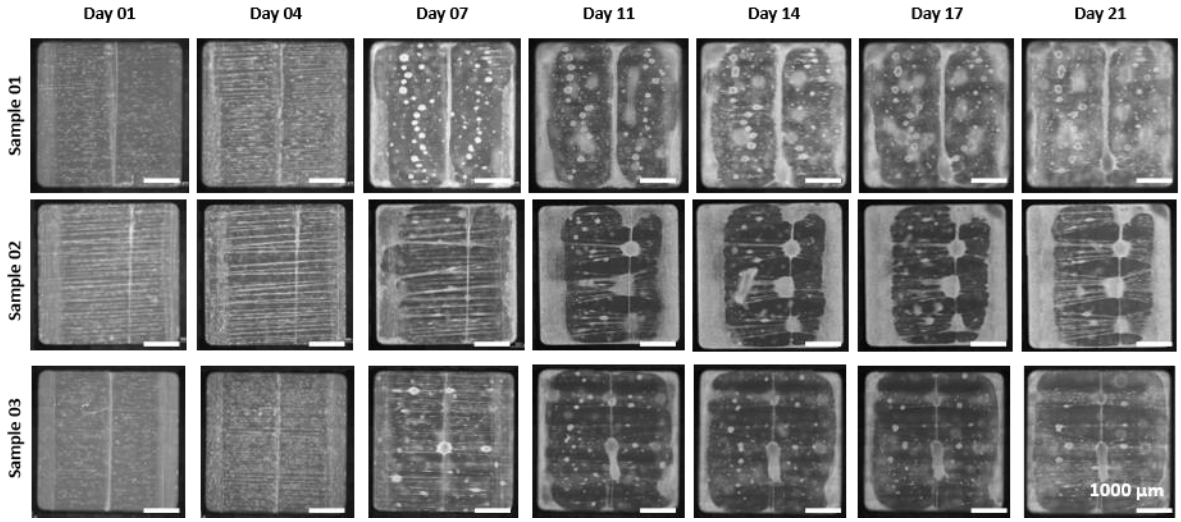

Figure 32: Mosaic images of pericytes seeded on 200 nm fiber networks with regions of aligned fibers in the horizontal direction and a central 2 µm base fiber.

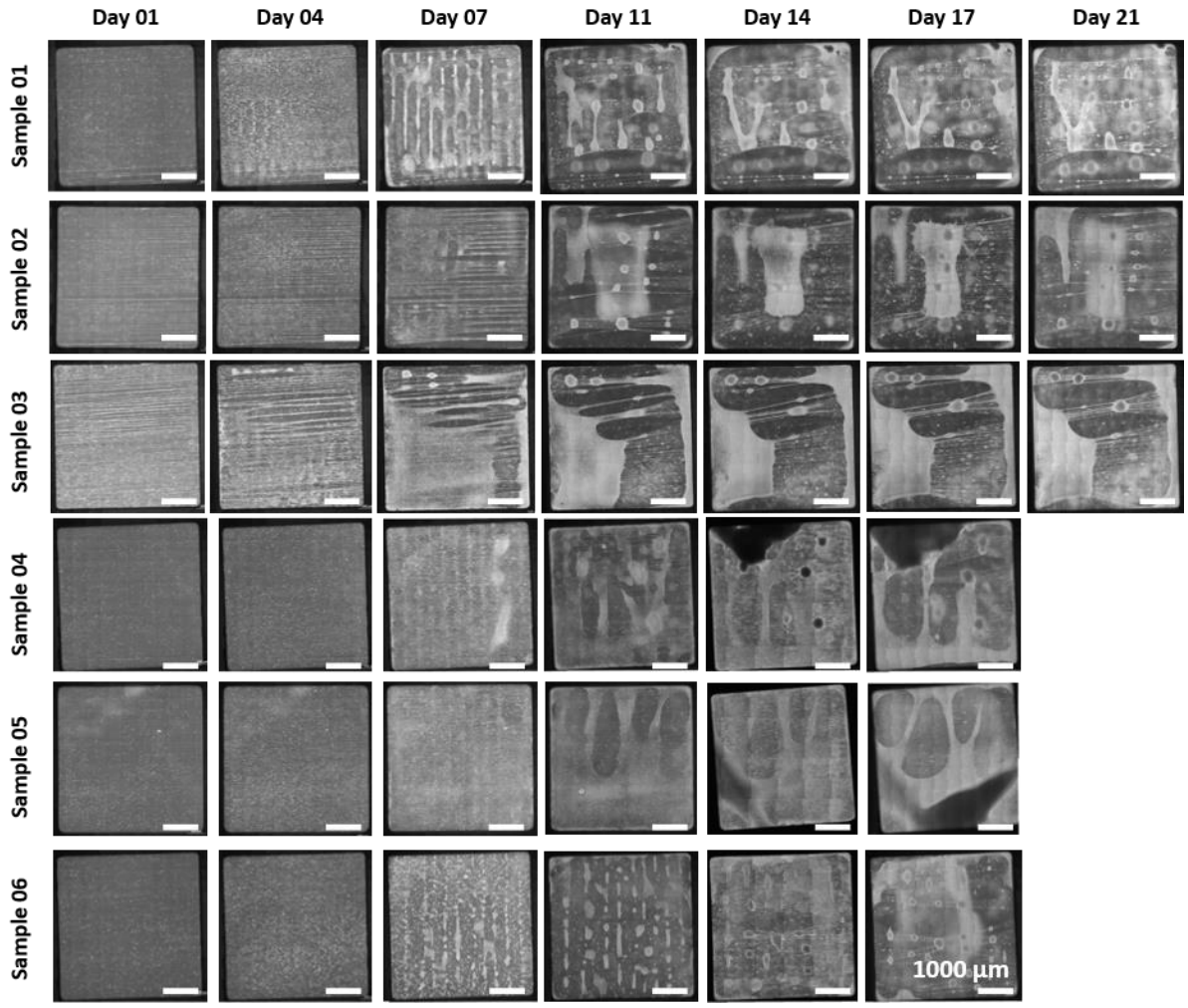

Figure 33: Mosaic images of pericytes seeded on 200 nm aligned fiber networks with 200 nm fibers in the vertical direction instead of the 2 µm base fiber.

3 Discussion

Mechanical signals from the microenvironment can impact cellular behavior.[57,58] The tissue's native extracellular matrix (ECM) is composed of protein fibers of varying stiffness and diameter,[54,59] which are altered during multiple processes such as migration,[60] tumor progression,[61–63] and tissue homeostasis.[64] Matrix stiffness has been found to alter spheroid shape and behavior, such as disaggregation of ovarian cancer cell spheroids[37] and increasing the invasiveness of pericytes and melanoma cell spheroids.[14,18] In this study, we show that biophysical factors like matrix stiffness (through changes in the fiber diameter) and fiber network architecture also impact the formation, growth, and behavior of pericyte spheroids.

The mechanical characteristics of spheroids can also be impacted by fiber matrices. For instance, malignant breast cancer cell spheroids show a rise in area and a drop in stiffness when treated with collagenase to dissolve collagen fibers within them.[65] Prior research with Hepatoma cell spheroid formation has revealed the distinct role of the ECM via integrin-ECM binding in the presence of fibrous matrices to stimulate spheroid formation via rapid aggregation followed by E-cadherin upregulation and cell-cell adhesion.[17,66] Here, our study evaluated pericyte spheroid formation in fibrous matrices and found that cells seem to pick up biophysical cues from the underlying networks for spheroid formation. We observed that fiber diameter in crosshatched networks influences pericytes to grow into either spheroids or monolayers. Aligned fiber networks, being easier to remodel with fewer fused junctions, facilitated spheroid formation on all diameters. Here, changes in diameter affected the way cells aggregate, resulting in different spheroid sizes

and shapes. Thus, when fiber networks were designed to have regions of small diameter aligned fibers and large diameter crosshatched fibers at different regions, we could spatially control the growth of pericytes into spheroids and monolayers within a scaffold. Spheroid occurrences were associated with extensive fiber remodeling while monolayers generally had intact fiber networks underneath them. Hence, the fiber architecture, stiffness, and cells' ability to remodel fibers appear to be critical factors in pericyte spheroid formation and behavior.

Collective cell migration is a mode of cell movement seen in processes such as morphogenesis, wound healing, and tumors.[67–71] With varying substrate stiffness, collective cell migration has been shown to have different characteristics by Beaune *et al*. with murine sarcoma cells.[26] Previously, we demonstrated migration of leader and follower cells in single, chain, and collective modes from a monolayer interfaced with aligned and crosshatched fiber networks.[71] On the aligned fiber networks, leader cells were seen to drag (pull) some spheroids during migration, similar to collective cell migration initiated by leader/tip cells.[72–75] We also observed instances of spheroids migrating without being pulled by a leader cell, due to potential difficulties in identifying a leader cell or the spheroids utilizing a coordinated mode with internal signaling. The ability of leader cells to pull spheroids suggests a sliding mode possible only on parallel fiber arrangements. Confocal images showed spheroid formation around fibers (i.e., fibers were noted within spheroids which made it surprising that spheroids were able to migrate on aligned fiber networks. As the spheroids grew, they remodeled the surrounding fibers and were mostly stationary. Spheroids in crosshatched fiber networks were also mostly stationary due to loss of fiber alignment during early formation.

Spheroids were non-migratory on the base fibers of aligned fiber networks, which were orthogonal and stiffer than the dense, aligned fibers. These observations suggest the influence of both stiffness and fiber architecture on spheroid migration.

The mechanical force exertions emerging from spheroids and responses when external forces are applied on it are a focal point of active research.[16,38,76,77] These forces help the cells remodel the surrounding fibrous environment and align the fibers and influence multicellular behavior.[15,19,38,76] Multiple techniques which track the deformation of the matrix, the displacement of microbeads, cantilevers, or microtweezers have been used to study spheroid forces.[19,38,65,76,78–80] We measured the dynamic forces that the spheroid exerted on fiber scaffolds during different interactions. At the start of spheroid formation, cells collectively applied a significant force on the scaffold. However, as the cells formed the spheroid, the net force decreased considerably as some cells detached from the fibers in the 2D plane and formed structures in 3D. The contracting cells also pulled the fibers along with them during formation. Decreased forces were also observed when single cells detached from the spheroid, highlighting the collective role of individual cells in exerting spheroid forces. Factors such as stiffness, matrix alignment, and fiber tension have been shown to increase invasiveness and sprouting in endothelial and melanoma cells spheroids.[15,18,81] Our fiber networks, which have highly aligned fibers in tension, provide an ideal tool for studying the merging and sprouting of cells from spheroids. Our findings showed that more cells sprouted from the spheroids compared to the number of cells that merged into spheroids. The spheroid area remained constant while cells were moving out of the spheroid, suggesting that the cells within the spheroid were dividing at a similar rate.

Pericyte contractility helps restructure vessel wall and regulate fluid flow in the microvasculature as they wrap around blood vessels.[41] Here, we show that the contractility of pericytes plays a significant role in their formation into 3D structures and can change their morphology upon inhibition. Feng *et al.*[14] showed that an increase in substrate stiffness can cause pericytes to transform into more invasive and mobile stromal fibroblasts (found primarily in solid tumors), impacting tumor angiogenesis, metastasis, and intravasation. On 3D fiber networks, dense, stiff matrices which mimic the tumor microenvironment inhibit the 3D aggregation of pericytes and influence tumor angiogenesis and metastasis via intravasation. Actin-myosin contractility has been shown to influence spheroid behavior and compaction in multiple cell types such as breast and ovarian cancer cells, human mesenchymal stem cells.[37,82,83] Inhibiting actin-myosin contractility via ROCK inhibition shows a reversible destabilizing effect on pericyte spheroids, and prolonged inhibition prior to seeding prevents pericytes from forming spheroidal structures, with monolayer formation being preferred instead. Thus, our findings indicate that contractility is a key factor in pericyte formation into 3D structures and its inhibition can affect their morphology and impact other putative functions.

According to Peyton *et al.*[84] smooth muscle cells (SMCs) with active RhoA demonstrated increased levels of f-actin bundling and vinculin expression. Additionally, the expression of contractile markers, such as α-actin and calponin, was also increased in these SMCs and were also dependent on the stiffness of the matrix. The *Acta2* gene, responsible for encoding smooth muscle α-actin, plays a crucial role in multiple mechanosensing aspects such as the cell's ability to contract and remodel the matrix and recruitment of integrins at cell-matrix adhesions.[85] Gene expression studies on small diameter (200 nm) aligned

fibers revealed that the expression of *Acta2* mimicked the changing number of spheroids, indicating its importance in maintaining their structure and function. The genes *Cnn1*, *Sm22*, and *Smtn*, also important in the pericyte/smooth muscle cell lineage, showed high expression during the early stages of spheroid formation, implying a key role in their 3D aggregation into spheroids.

4 Conclusions

In conclusion, our findings show that the STEP fiber networks can be tuned to multiple configurations by changing the architecture and stiffness to examine the effect of mechanical signals on pericyte behavior in fiber-based environments. Pericytes adapt to the fiber diameter and architecture and manipulate the fiber networks to dictate their aggregation into 3D spheroids or 2D monolayers. Further research can be done to delve deeper into the dynamics of pericyte spheroid interactions with suspended fiber networks, exploring the correlation between diameter, stiffness, architecture, and their interaction with cells/spheroid in these matrices to understand the crucial role the microenvironment plays in the culture and growth of spheroids.

5 Limitations and future scope

In the current study, we probed how changing different mechanical properties of the fiber networks can influence pericyte cell aggregation. To simplify the study, and to get an overview of these effects, we used two different fiber networks, three different fiber diameters within these networks, and kept the spacing between the fibers the same (10-15 μm). We would like to extend this study by also looking at how the interfiber spacing in both architectures plays a role in pericyte aggregation in spheroids. Larger spacing would

lead to fewer fused junctions and a decreased stiffness (with increase in length between the fused junctions), implying easier remodeling of the fiber networks. Seeding the pericytes in new architectures and introducing variations with diameter of the base fibers of the aligned networks can also be probed to better understand the role of fiber architecture and diameter. There are a lot more effects in play here, which were not picked up with our current study, as we saw with the variation in the aggregation and behavior of pericytes with 500 nm aligned fibers when compared to 200 and 800 nm aligned fibers.

We also observed multiple dynamic interactions with our fiber networks which we report here. Most of these studies were done with 200 nm aligned and crosshatched networks due to ease of manufacturing and great repeatability the spheroid fromations. These studies can be extended to other diameters as well, and one can question how the diameter influences their behavior and their interactions with their surrounding environment.

While we show that spheroids do form with pericytes derived from different locations in the body and from different patients, all our studies were done with one particular patient cell line. Is this behavior specific to the location/patient? A more comprehensive study should be done and the repeatability of the results from one pericyte cell line should be checked against other pericyte cell lines derived from both different locations as well as patients.

Since pericytes are generally found with endothelial cells (ECs), we can also extend this study to ECs as well. Do ECs aggregate on STEP fiber networks as well? How would the different fiber architectures and diameters influence their aggregation and behavior? And

more importantly, what would happen if ECs and pericytes were cocultured, as seen *in vivo* in the microvasculature? How would they assemble and what kind of aggregates would these cocultures form? Our work here has laid the foundation to probe many of these questions and can lead to a better understanding of various events in the microvasculature and during angiogenesis.

References

1. Pedersen, J. A. & Swartz, M. A. Mechanobiology in the third dimension. *Ann. Biomed. Eng.* **33**, 1469–1490 (2005).
2. Sakalem, M. E., De Sibio, M. T., da Costa, F. A. da S. & de Oliveira, M. Historical evolution of spheroids and organoids, and possibilities of use in life sciences and medicine. *Biotechnology Journal* vol. 16 2000463 (2021).
3. Zanoni, M. *et al.* Modeling neoplastic disease with spheroids and organoids. *Journal of Hematology and Oncology* vol. 13 (2020).
4. Ong, C. S. *et al.* In vivo therapeutic applications of cell spheroids. *Biotechnology Advances* vol. 36 494–505 (2018).
5. Achilli, T. M., Meyer, J. & Morgan, J. R. Advances in the formation, use and understanding of multi-cellular spheroids. *Expert Opinion on Biological Therapy* vol. 12 1347–1360 (2012).
6. Kim, S. jeong, Kim, E. M., Yamamoto, M., Park, H. & Shin, H. Engineering Multi-Cellular Spheroids for Tissue Engineering and Regenerative Medicine. *Advanced Healthcare Materials* vol. 9 (2020).
7. Duval, K. *et al.* Modeling physiological events in 2D vs. 3D cell culture. *Physiology* vol. 32 266–277 (2017).

8. Baker, B. M. & Chen, C. S. Deconstructing the third dimension-how 3D culture microenvironments alter cellular cues. *Journal of Cell Science* vol. 125 3015–3024 (2012).

9. Shao, C. *et al.* Development of Cell Spheroids by Advanced Technologies. *Advanced Materials Technologies* vol. 5 2000183 (2020).

10. Mueller-Klieser, W. Multicellular spheroids - A review on cellular aggregates in cancer research. *Journal of Cancer Research and Clinical Oncology* vol. 113 101–122 (1987).

11. Kelm, J. M., Timmins, N. E., Brown, C. J., Fussenegger, M. & Nielsen, L. K. Method for generation of homogeneous multicellular tumor spheroids applicable to a wide variety of cell types. *Biotechnol. Bioeng.* **83**, 173–180 (2003).

12. Ruedinger, F., Lavrentieva, A., Blume, C., Pepelanova, I. & Scheper, T. Hydrogels for 3D mammalian cell culture: a starting guide for laboratory practice. *Applied Microbiology and Biotechnology* vol. 99 623–636 (2015).

13. Youssef, J., Nurse, A. K., Freund, L. B. & Morgan, J. R. Quantification of the forces driving self-assembly of three-dimensional microtissues. *Proc. Natl. Acad. Sci. U. S. A.* **108**, 6993–6998 (2011).

14. Feng, F., Feng, X., Zhang, D., Li, Q. & Yao, L. Matrix Stiffness Induces Pericyte-Fibroblast Transition Through YAP Activation. *Front. Pharmacol.* **12**, 1370 (2021).

15. Korff, T. & Augustin, H. G. Tensional forces in fibrillar extracellular matrices control directional capillary sprouting. *J. Cell Sci.* **112**, 3249–3258 (1999).

16. Boot, R. C., Koenderink, G. H. & Boukany, P. E. Spheroid mechanics and

implications for cell invasion. *Advances in Physics: X* vol. 6 (2021).

17. Efremov, Y. M. *et al.* Mechanical properties of cell sheets and spheroids: the link between single cells and complex tissues. *Biophysical Reviews* vol. 13 541–561 (2021).
18. Ahmadzadeh, H. *et al.* Modeling the two-way feedback between contractility and matrix realignment reveals a nonlinear mode of cancer cell invasion. *Proc. Natl. Acad. Sci. U. S. A.* **114**, E1617–E1626 (2017).
19. Kopanska, K. S., Alcheikh, Y., Staneva, R., Vignjevic, D. & Betz, T. Tensile forces originating from cancer spheroids facilitate tumor invasion. *PLoS One* **11**, (2016).
20. Blacher, S. *et al.* Cell invasion in the spheroid sprouting assay: A spatial organisation analysis adaptable to cell behaviour. *PLoS One* **9**, e97019 (2014).
21. Tevis, K. M., Colson, Y. L. & Grinstaff, M. W. Embedded Spheroids as Models of the Cancer Microenvironment. *Adv. Biosyst.* **1**, (2017).
22. Gunay, G. *et al.* The effects of size and shape of the ovarian cancer spheroids on the drug resistance and migration. *Gynecol. Oncol.* **159**, 563–572 (2020).
23. Dean, Z. S., Elias, P., Jamilpour, N., Utzinger, U. & Wong, P. K. Probing 3D collective cancer invasion using double-stranded locked nucleic acid biosensors. *Anal. Chem.* **88**, 8902–8907 (2016).
24. Dey, M., Ayan, B., Yurieva, M., Unutmaz, D. & Ozbolat, I. T. Studying Tumor Angiogenesis and Cancer Invasion in a Three-Dimensional Vascularized Breast Cancer Micro-Environment. *Adv. Biol.* **5**, 2100090 (2021).
25. Higgins, G. *et al.* An exploratory study on the role of the stiffness of breast cancer

cells in their detachment from spheroids and migration in 3D collagen matrices. *BioRxiv* 2001–2021 (2022) doi:10.1101/2021.01.21.427639.

26. Beaune, G. *et al.* Spontaneous migration of cellular aggregates from giant keratocytes to running spheroids. *Proc. Natl. Acad. Sci. U. S. A.* **115**, 12926–12931 (2018).

27. Cui, H. *et al.* Assembly of Multi-Spheroid Cellular Architectures by Programmable Droplet Merging. *Adv. Mater.* **33**, 2006434 (2021).

28. Schneider, O. *et al.* Fusing spheroids to aligned μ-tissues in a heart-on-chip featuring oxygen sensing and electrical pacing capabilities. *Mater. Today Bio* **15**, (2022).

29. Bratt-Leal, A. M., Kepple, K. L., Carpenedo, R. L., Cooke, M. T. & McDevitt, T. C. Magnetic manipulation and spatial patterning of multi-cellular stem cell aggregates. *Integr. Biol.* **3**, 1224–1232 (2011).

30. Zhao, L., Liu, Y., Liu, Y., Zhang, M. & Zhang, X. Microfluidic Control of Tumor and Stromal Cell Spheroids Pairing and Merging for Three-Dimensional Metastasis Study. *Anal. Chem.* **92**, 7638–7645 (2020).

31. Ahmed, H. M. M. *et al.* Human liver microtissue spheroids in hollow fiber membrane bioreactor. *Colloids Surfaces B Biointerfaces* **160**, 272–280 (2017).

32. Gómez-González, M., Latorre, E., Arroyo, M. & Trepat, X. Measuring mechanical stress in living tissues. *Nat. Rev. Phys.* **2**, 300–317 (2020).

33. Baker, B. M. *et al.* Cell-mediated fibre recruitment drives extracellular matrix mechanosensing in engineered fibrillar microenvironments. *Nat. Mater.* **14**, 1262–1268 (2015).

34. Shin, J. Y. *et al.* Efficient formation of cell spheroids using polymer nanofibers. *Biotechnol. Lett.* **34**, 795–803 (2012).

35. Wei, J., Lu, J., Liu, Y., Yan, S. & Li, X. Spheroid culture of primary hepatocytes with short fibers as a predictable in vitro model for drug screening. *J. Mater. Chem. B* **4**, 7155–7167 (2016).

36. Ahmad, T. *et al.* Hybrid-spheroids incorporating ECM like engineered fragmented fibers potentiate stem cell function by improved cell/cell and cell/ECM interactions. *Acta Biomater.* **64**, 161–175 (2017).

37. McKenzie, A. J. *et al.* The mechanical microenvironment regulates ovarian cancer cell morphology, migration, and spheroid disaggregation. *Sci. Rep.* **8**, 1–20 (2018).

38. Mark, C. *et al.* Collective forces of tumor spheroids in three-dimensional biopolymer networks. *Elife* **9**, (2020).

39. Gerhardt, H. & Betsholtz, C. Endothelial-pericyte interactions in angiogenesis. *Cell and Tissue Research* vol. 314 15–23 (2003).

40. Armulik, A., Abramsson, A. & Betsholtz, C. Endothelial/pericyte interactions. *Circulation Research* vol. 97 512–523 (2005).

41. Dessalles, C. A., Babataheri, A. & Barakat, A. I. Pericyte mechanics and mechanobiology. *Journal of Cell Science* vol. 134 (2021).

42. Billaud, M. *et al.* Classification and Functional Characterization of Vasa Vasorum-Associated Perivascular Progenitor Cells in Human Aorta. *Stem Cell Reports* **9**, 292–303 (2017).

43. Kumarasamy, M. & Sosnik, A. Heterocellular spheroids of the neurovascular blood-brain barrier as a platform for personalized nanoneuromedicine. *iScience* **24**,

102183 (2021).

44. Cho, C. F. *et al.* Blood-brain-barrier spheroids as an in vitro screening platform for brain-penetrating agents. *Nat. Commun.* **8**, 1–14 (2017).

45. Urich, E. *et al.* Multicellular self-assembled spheroidal model of the blood brain barrier. *Sci. Rep.* **3**, 1–8 (2013).

46. Wang, Y. C. *et al.* Notch1 promotes the pericyte-myofibroblast transition in idiopathic pulmonary fibrosis through the PDGFR/ROCK1 signal pathway. *Exp. Mol. Med.* **51**, 1–11 (2019).

47. Vakhrushev, I. V. *et al.* Heterotypic multicellular spheroids as experimental and preclinical models of sprouting angiogenesis. *Biology (Basel).* **11**, 1–20 (2022).

48. Nain, A. S., Sitti, M., Jacobson, A., Kowalewski, T. & Amon, C. Dry spinning based spinneret based tunable engineered parameters (STEP) technique for controlled and aligned deposition of polymeric nanofibers. *Macromol. Rapid Commun.* **30**, 1406–1412 (2009).

49. Wintruba, K. L. *et al.* Adventitia-Derived Extracellular Matrix Hydrogel Enhances Contractility of Human Vasa Vasorum-Derived Pericytes via α2β1 integrin and TGFβ Receptor. *J. Biomed. Mater. Res. - Part A* **110**, 1912–1920 (2022).

50. Sheets, K., Wang, J., Zhao, W., Kapania, R. & Nain, A. S. Nanonet Force Microscopy for Measuring Cell Forces. *Biophys. J.* **111**, 197–207 (2016).

51. Hall, A. *et al.* Nanonet force microscopy for measuring forces in single smooth muscle cells of the human aorta. *Mol. Biol. Cell* **28**, 1894–1900 (2017).

52. Padhi, A. *et al.* Cell Fragment Formation, Migration, and Force Exertion on Extracellular Mimicking Fiber Nanonets. *Adv. Biol.* **5**, 2000592 (2021).

53. Padhi, A. *et al.* Force-exerting perpendicular lateral protrusions in fibroblastic cell contraction. *Commun. Biol.* **3**, 1–11 (2020).

54. Smith, L. A. & Ma, P. X. Nano-fibrous scaffolds for tissue engineering. *Colloids Surfaces B Biointerfaces* **39**, 125–131 (2004).

55. Hussey, G. S., Dziki, J. L. & Badylak, S. F. Extracellular matrix-based materials for regenerative medicine. *Nat. Rev. Mater.* **3**, 159–173 (2018).

56. Jana, A. *et al.* Sculpting Rupture-Free Nuclear Shapes in Fibrous Environments. *Adv. Sci.* **9**, 2203011 (2022).

57. Padhi, A. & Nain, A. S. ECM in Differentiation: A Review of Matrix Structure, Composition and Mechanical Properties. *Annals of Biomedical Engineering* vol. 48 1071–1089 (2020).

58. Wei, Q. *et al.* Cellular modulation by the mechanical cues from biomaterials for tissue engineering. *Biomater. Transl.* **2**, 323 (2021).

59. Wade, R. J. & Burdick, J. A. Engineering ECM signals into biomaterials. *Materials Today* vol. 15 454–459 (2012).

60. Van Helvert, S. & Friedl, P. Strain Stiffening of Fibrillar Collagen during Individual and Collective Cell Migration Identified by AFM Nanoindentation. *ACS Applied Materials and Interfaces* vol. 8 21946–21955 (2016).

61. Radisky, D., Muschler, J. & Bissell, M. J. Order and disorder: The role of extracellular matrix in epithelial cancer. in *Cancer Investigation* vol. 20 139–153 (2002).

62. Lu, P., Weaver, V. M. & Werb, Z. The extracellular matrix: A dynamic niche in cancer progression. *Journal of Cell Biology* vol. 196 395–406 (2012).

63. Taubenberger, A. V. *et al.* 3D extracellular matrix interactions modulate tumour cell growth, invasion and angiogenesis in engineered tumour microenvironments. *Acta Biomater.* **36**, 73–85 (2016).

64. Ford, A. J. & Rajagopalan, P. Extracellular matrix remodeling in 3D: implications in tissue homeostasis and disease progression. *Wiley Interdiscip. Rev. Nanomedicine Nanobiotechnology* **10**, e1503 (2018).

65. Jaiswal, D. *et al.* Stiffness analysis of 3D spheroids using microtweezers. *PLoS One* **12**, (2017).

66. Lin, R. Z., Chou, L. F., Chien, C. C. M. & Chang, H. Y. Dynamic analysis of hepatoma spheroid formation: Roles of E-cadherin and β1-integrin. *Cell Tissue Res.* **324**, 411–422 (2006).

67. Christiansen, J. J. & Rajasekaran, A. K. Reassessing epithelial to mesenchymal transition as a prerequisite for carcinoma invasion and metastasis. *Cancer Research* vol. 66 8319–8326 (2006).

68. Friedl, P. & Gilmour, D. Collective cell migration in morphogenesis, regeneration and cancer. *Nature Reviews Molecular Cell Biology* vol. 10 445–457 (2009).

69. Scarpa, E. & Mayor, R. Collective cell migration in development. *J. Cell Biol.* **212**, 143–155 (2016).

70. Poujade, M. *et al.* Collective migration of an epithelial monolayer in response to a model wound. *Proc. Natl. Acad. Sci. U. S. A.* **104**, 15988–15993 (2007).

71. Sharma, P. *et al.* Aligned fibers direct collective cell migration to engineer closing and nonclosing wound gaps. *Mol. Biol. Cell* **28**, 2579–2588 (2017).

72. Haeger, A., Wolf, K., Zegers, M. M. & Friedl, P. Collective cell migration:

Guidance principles and hierarchies. *Trends in Cell Biology* vol. 25 556–566 (2015).

73. Carey, S. P., Starchenko, A., McGregor, A. L. & Reinhart-King, C. A. Leading malignant cells initiate collective epithelial cell invasion in a three-dimensional heterotypic tumor spheroid model. *Clin. Exp. Metastasis* **30**, 615–630 (2013).
74. Khalil, A. A. & Friedl, P. Determinants of leader cells in collective cell migration. *Integrative Biology* vol. 2 568–574 (2010).
75. Mayor, R. & Etienne-Manneville, S. The front and rear of collective cell migration. *Nature Reviews Molecular Cell Biology* vol. 17 97–109 (2016).
76. Lee, W. *et al.* Dispersible hydrogel force sensors reveal patterns of solid mechanical stress in multicellular spheroid cultures. *Nat. Commun.* **10**, 1–14 (2019).
77. Blumlein, A., Williams, N. & McManus, J. J. The mechanical properties of individual cell spheroids. *Sci. Rep.* **7**, (2017).
78. Jaiswal, D., Moscato, Z., Tomizawa, Y., Claffey, K. P. & Hoshino, K. Elastography of multicellular spheroids using 3D light microscopy. *Biomed. Opt. Express* **10**, 2409 (2019).
79. Zanetti, M., Andolfi, L., Taylor, M. R. G., Mestroni, L. & Lazzarino, M. AFM macro-probes to investigate whole 3D cardiac spheroids. *Micro Nano Eng.* **15**, 100134 (2022).
80. Valencia, A. M. J. *et al.* Collective cancer cell invasion induced by coordinated contractile stresses. *Oncotarget* **6**, 43438–43451 (2015).
81. Crosby, C. O. & Zoldan, J. Mimicking the physical cues of the ECM in angiogenic

biomaterials. *Regen. Biomater.* **6**, 61–73 (2019).

82. Tsai, A. C., Liu, Y., Yuan, X. & Ma, T. Compaction, fusion, and functional activation of three-dimensional human mesenchymal stem cell aggregate. *Tissue Eng. - Part A* **21**, 1705–1719 (2015).

83. Devanny, A. J., Vancura, M. B. & Kaufman, L. J. Exploiting differential effects of actomyosin contractility to control cell sorting among breast cancer cells. *Mol. Biol. Cell* **32**, ar24 (2021).

84. Peyton, S. R., Kim, P. D., Ghajar, C. M., Seliktar, D. & Putnam, A. J. The effects of matrix stiffness and RhoA on the phenotypic plasticity of smooth muscle cells in a 3-D biosynthetic hydrogel system. *Biomaterials* **29**, 2597–2607 (2008).

85. Massett, M. P. *et al.* Loss of smooth muscle α-actin effects on mechanosensing and cell–matrix adhesions. *Exp. Biol. Med.* **245**, 374–384 (2020).